Dynamical Stability and Quantum Chaos of Ions in a Linear Trap

G.P. Berman [1] ¹, D.F.V. James [2], R.J. Hughes [3], M.S. Gulley [4], M.H. Holzscheiter [3]

[1] Group T-13 and CNLS, [2] Group T-4, [3] Group P-23, [4] Group P-25 University of California, Los Alamos National Laboratory Los Alamos, NM87545, USA

> and G.V. López

Departamento de Física, Universidad de Guadalajara Corregidora 500, S.R. 44420, Guadalajara, Jalisco, Mexico

to be submitted to Physical Review A

Abstract

The realization of a paradigm chaotic system, namely the harmonically driven oscillator, in the quantum domain using cold trapped ions driven by lasers is theoretically investigated. The simplest characteristics of regular and chaotic dynamics are calculated. The possibilities of experimental realization are discussed.

PACS numbers:42.50.Vk, 05.45.Mt, 32.80.Pj LA-UR-99-1217

¹Address correspondence to Dr. G.P. Berman, Theoretical Division T-13, MS B-213, Los Alamos National Laboratory, Los Alamos NM 87545, USA. Email gpb@lanl.gov.

1 Introduction

One of the major difficulties in developing quantum technologies, such as quantum computers [1, 2], are the different kinds of specifically quantum dynamical instabilities that can occur due to interactions between different degrees of freedom and resonant interaction with the external fields. These instabilities differ from dynamical instabilities in classical systems, which are usually connected with strong dependence of trajectories on the initial conditions and on the values of parameters. Small variations of initial conditions or parameters lead to large deviations in time of the corresponding trajectories. If the speed of this deviation is exponential, the system becomes chaotic, and the appropriate methods of description are statistical rather than deterministic. But for quantum systems, the notion of a trajectory is not well defined. This is one of the main reasons why most of the well-developed methods for stability analysis can not be directly applied to quantum systems. Moreover, as was first shown theoretically by Berman and Zaslavsky [3, 4] (see also [5]), even in a "deep" quasiclassical region, classically chaotic systems can have quantum dynamics that is very different from the corresponding classical dynamics.

Another important phenomenon which takes place in quantum systems which are classically chaotic is quantum nonlinear resonance (QNR), which was first introduced and investigated theoretically by Berman and Zaslavsky [6]. QNRs are quantum manifestation of nonlinear resonances which play very important role in classically chaotic systems [7]-[10]. Interactions of QNRs are known to be intimately connected to the transition to quantum chaos [11]-[17]. In the simplest situations, QNRs occur when a bound quantum system whose energy levels are not equally spaced is driven by a resonant perturbation. A QNR is characterized by two main parameters: the number of quasi-energy levels, δn , which are "trapped" in the potential well of the resonance, and the characteristic frequency of slow phase oscillations, Ω_{ph} . Isolated QNRs imply stable quantum dynamics; overlapping QNRs cause a transition to quantum chaos. QNRs are very general phenomena in non-integrable quantum systems, and can be thought of as "quasi-particles" of quantum chaos (for more details, see chapter 9 of Reichl's recent book [18], which is devoted to the transition to quantum chaos caused by interaction of QNRs). Until now, QNR effects have been experimentally investigated using Rydberg atoms in a resonant micro-wave field [19]. Understanding the instabilities connected with overlapping QNRs is important for fundamental problems related to the transition to quantum chaos, and for the design of experimental devices (such as quantum computers based on ion traps) in which these instabilities may cause significant problems. To study the characteristic parameters of both isolated QNR's and the problems related to interaction of QNRs it is important to choose a model which (a) involves regulated (and relatively small) number of interacting QNRs; (b) can be implemented experimentally in quantum and quasiclassical regions of parameters.

In this paper we introduce a quantum model which is convenient for investigation of quantum dynamical instabilities and transition to quantum chaos based on overlapping of QNRs. The model consists of a single ion confined in a radio-frequency Paul trap and which interacts with a resonant laser field. In the classical limit, this model reduces to the well-known model of a linear oscillator interacting with a plane electromagnetic wave, and was investigated in [20] (see also references therein). The main advantage of our model is that the number of interacting QNRs can be regulated, for example, by varying the intensity of the laser radiation, which is difficult to achieve in other models based on the kicked interaction [24]-[28].

Devices based on trapped ions have been used to investigate experimentally fundamental aspects of quantum mechanics [29, 30], as well as for important technological applications such as optical frequency standards [31] and quantum computing [1, 32]. Ions are confined by a combination of a rotating quadrupole potential (induced by the rod electrodes) and a weak electrostatic potential (induced by the conical endcap electrodes). The ions, once trapped, can be cooled by standard Doppler cooling and by a optical pumping method ("sideband cooling"), which can cool multiple ions down to the quantum mechanical ground state of the trapping potential. In an ion trap quantum computer, information can be stored in the internal quantum states of the ions (which constitute the quantum bits, or "qubits" of the computer), and, using ultra narrow bandwidth lasers, quantum gate operations can be realized between pairs of qubits using quantum states of the collective motion of the ions in the harmonic confining potential as a quantum information bus [33]. As such devices are specifically designed to investigate experimentally the preparation, evolution and measurement of quantum systems with large dimension Hilbert spaces, the linear ion trap is an ideal apparatus to investigate the problems of quantum dynamical stability, the transition to quantum chaos, and the spectroscopy of quantum nonlinear resonances. In this paper, we present the main elements of the derivation of our model – a quantum linear oscillator driven by a monochromatic wave, and the preliminary analytical and numerical results on the classical and quantum dynamics in different regions of parameters.

The paper is organized as follows. In section 2, the theory of how a trapped ion can be driven by laser fields in the manner of the harmonically driven oscillator is

described in detail. It should be noted in particular how similar the arrangement and laser requirements are to those employed in ion trap quantum computer experiments. In section 3, the *classical* theory of the harmonically driven oscillator is discussed; the quantum theory is described in section 4. The connection of this system with the solid-state Anderson localization model is described in section 5. The results of numerical simulations are presented in section 6. We conclude this paper with a brief discussion of the possibilities for experimental verifications.

2 Raman interactions of lasers and trapped ions

A single ion confined in a linear radio-frequency (rf) trap may be described by an effective Hamiltonian given by the formula [33]

$$\hat{H} = \frac{1}{2m}\hat{p}^2 + \frac{1}{2}m\omega^2\hat{x}^2 + \hat{H}_I,\tag{2.1}$$

where m is the mass of the ion, \hat{x} (\hat{p}) is the position (momentum) operator for the ion and ω is the angular trapping frequency. We are only considering motion of the ion along one direction, namely the axis of weak confinement of the trap; the ion is strongly confined along the other two directions, transverse to the axis and so we will assume that the motion in those directions can be neglected (see Fig.1).

We will employ the interference of two laser beams acting on the ion to realize experimentally our desired interaction Hamiltonian \hat{H}_I . Such Raman interactions between lasers and ions are a standard technique, and are described in detail elsewhere [34]. The ion, confined in the harmonic trapping potential, will have many quantum levels associated with both the internal (atomic) variables and the external (motional) degrees of freedom. We will confine our attention two manifolds of such states, separated in energy by an appreciable amount (see Fig.2). What we have in mind is a lower manifold consisting of the magnetic sublevels of our ion, each level having a series of sidebands associated with excitation of quanta of the external harmonic oscillations; the upper manifold would then be the sublevels of an excited state of the ion, with similar sidebands. The lasers with which the ion is interacting will be detuned from the optical transition between the upper and lower levels, so that there is a negligible probability of any of these levels becoming excited: the lasers only cause redistribution of population amongst the lower manifold of levels. The upper levels may then be adiabatically eliminated from the problem, and one can therefore show that the matrix elements of the effective interaction Hamiltonian for the lower manifold is given by the formula [34]

$$\langle M|\hat{H}_I|N\rangle = -\sum_L \sum_{\alpha,\alpha'} \frac{\Omega_{ML}^{(\alpha)} \Omega_{NL}^{(\alpha')*}}{4\hbar(\omega_L - \omega_N - \omega_{\alpha'})} \exp\left[i\left(\omega_\alpha - \omega_{\alpha'}\right)t\right],\tag{2.2}$$

where the sum involving u is over all of the upper manifold levels and the two sums involving α and α' are over all of the applied laser fields, the Rabi frequency of the α -th laser being defined by

$$\hbar\Omega_{ML}^{(\alpha)} = \langle M|\hat{d}_i E_i^{(\alpha)}(\hat{\mathbf{r}})|L\rangle. \tag{2.3}$$

In Eq. (2.3), \hat{d}_i is the *i*-th component of the dipole moment operator (i = (1, 2, 3), standing for the three Cartesian components of a vector, and summation over repeated indices being implied), $E_i^{(\alpha)}$ is the *i*-th component of the electric field from the α -th laser (which is a function of the ion's position operator, $\hat{\mathbf{r}}$), $\hbar\omega_M$ is the energy of the M-th lower manifold level, $\hbar\omega_L$ is the energy of the L-th upper manifold level, and ω_α is the angular frequency of the α -th laser.

To proceed, we will make the distinction between internal and external degrees of freedom. We can form a basis set for the Hilbert space from a tensor product of a set of internal quantum levels with a basis set for the external degrees of freedom (for example the Fock states of the Harmonic oscillator). The set of internal states will be divided between the upper and lower manifolds. Thus we will make the following substitution:

$$|L\rangle \rightarrow |\lambda\rangle|l\rangle$$
 (2.4)

$$|M\rangle \rightarrow |\mu\rangle|m\rangle$$
 (2.5)

$$|N\rangle \rightarrow |\nu\rangle|n\rangle,$$
 (2.6)

where $|m\rangle, |n\rangle$ and $|l\rangle$ are members of the basis states for the motion degrees of freedom, $|\lambda\rangle$ is a member of the upper internal manifold and $|\mu\rangle$ and $|\nu\rangle$ are members of the lower internal manifold. In this notation, the matrix elements of the Hamiltonian Eq. (2.2) become:

$$\langle \mu | \langle m | \hat{H}_{I} | n \rangle | \nu \rangle = -\sum_{\lambda} \sum_{l} \sum_{\alpha, \alpha'} \frac{\langle \mu | \hat{d}_{i} | \lambda \rangle \langle \lambda | \hat{d}_{j} | \nu \rangle}{4\hbar(\omega_{\lambda} - \omega_{\nu} - \omega_{\alpha'} + \omega_{l} - \omega_{n})} \times \langle m | E_{i}^{(\alpha)}(\hat{\mathbf{r}}) | l \rangle \langle l | E_{j}^{(\alpha')*}(\hat{\mathbf{r}}) | n \rangle \exp\left[i\left(\omega_{\alpha} - \omega_{\alpha'}\right) t\right]. \tag{2.7}$$

The average detuning of the λ -th upper manifold level is be defined to be

$$\Delta_{\lambda} = \omega_{\lambda} - \bar{\omega}_{\nu} - \bar{\omega}_{\alpha},\tag{2.8}$$

where $\hbar \bar{\omega}_{\nu}$ is the average energy of the lower manifold and $\bar{\omega}_{\alpha}$ is the average of the laser frequencies. We will assume that, in the denominator of the fraction appearing in Eq. (2.7), we can make the following approximation:

$$\omega_{\lambda} - \omega_{\nu} - \omega_{\alpha'} + \omega_l - \omega_n \approx \Delta_{\lambda}. \tag{2.9}$$

If we use the completeness property of the external basis states (i.e. $\sum_{l} |l\rangle\langle l| = \hat{I}$, where \hat{I} is the identity operator), then we obtain the following formula for the Hamiltonian operator for the lower manifold states:

$$\hat{H}_I = \sum_{\mu,\nu} \kappa_{\mu,\nu} \left(\hat{\mathbf{r}}, t \right) |\mu\rangle\langle\nu|, \qquad (2.10)$$

where

$$\kappa_{\mu,\nu}(\hat{\mathbf{r}},t) = -\sum_{\lambda} \frac{\langle \mu | \hat{d}_i | \lambda \rangle \langle \lambda | \hat{d}_j | \nu \rangle}{4\hbar \Delta_{\lambda}} E_i(\hat{\mathbf{r}},t) E_j^*(\hat{\mathbf{r}},t), \qquad (2.11)$$

and the total laser field E_i is the sum of the different laser components:

$$E_i(\hat{\mathbf{r}}, t) = \sum_{\alpha} E_i^{(\alpha)}(\hat{\mathbf{r}}) \exp(i\omega_{\alpha} t). \qquad (2.12)$$

2.1 Two level systems

Let us now assume that there are only two internal levels in the lower manifold, which we will denote $|1\rangle$ and $|2\rangle$. As will be discussed below, this is a reasonable assumption to make for the atomic systems we have in mind. Also, we introduce a special coordinate system: the two internal levels are split by a magnetic field acting along the Z axis, which is the axis of quantization for the internal levels of our ion. The other two axes are the X and Y axes. These axes do not necessarily coincide with the x, y, z directions introduced to describe the motion of the ion in the trap. In this case it is convenient to use the Pauli operators for the system:

$$\hat{\sigma}_1 = |1\rangle\langle 2| + |2\rangle\langle 1|, \qquad (2.13)$$

$$\hat{\sigma}_2 = i(|1\rangle\langle 2| - |2\rangle\langle 1|), \qquad (2.14)$$

$$\hat{\sigma}_3 = |2\rangle\langle 2| - |1\rangle\langle 1|. \tag{2.15}$$

Using these operators the Hamiltonian can be written as follows:

$$\hat{H}_{I} = h_{0}(\hat{\mathbf{r}}, t) \hat{I} + h_{i}(\hat{\mathbf{r}}, t) \hat{\sigma}_{i}, \qquad (2.16)$$

where \hat{I} is the identity operator $(|1\rangle\langle 1| + |2\rangle\langle 2|)$ and

$$h_0(\hat{\mathbf{r}},t) = \frac{1}{2} \left[\kappa_{1,1}(\hat{\mathbf{r}},t) + \kappa_{2,2}(\hat{\mathbf{r}},t) \right],$$
 (2.17)

$$h_1(\hat{\mathbf{r}},t) = \frac{1}{2} \left[\kappa_{1,2}(\hat{\mathbf{r}},t) + \kappa_{2,1}(\hat{\mathbf{r}},t) \right],$$
 (2.18)

$$h_2(\hat{\mathbf{r}},t) = \frac{1}{2i} \left[\kappa_{1,2}(\hat{\mathbf{r}},t) - \kappa_{2,1}(\hat{\mathbf{r}},t) \right],$$
 (2.19)

$$h_3(\hat{\mathbf{r}},t) = \frac{1}{2} \left[\kappa_{2,2}(\hat{\mathbf{r}},t) - \kappa_{1,1}(\hat{\mathbf{r}},t) \right].$$
 (2.20)

For the special case that the lower manifold of internal states consists of two magnetic sublevels of the ${}^2S_{1/2}$ ground state of an alkali-like ion, and the upper manifold is the two sublevels of the ${}^2P_{1/2}$ excited state whose Zeeman splitting is not too big, the atomic matrix elements appearing in Eq. (2.11) can be calculated in closed form. As a result the components of h appearing in Eq. (2.16) reduce to the following simple form (see appendix A):

$$h_{0}(\hat{\mathbf{r}},t) = -\chi |\mathbf{E}(\hat{\mathbf{r}},t)|^{2}$$

$$h_{1}(\hat{\mathbf{r}},t) = 2\chi \operatorname{Im} \{E_{Z}(\hat{\mathbf{r}},t) E_{Y}^{*}(\hat{\mathbf{r}},t)\}$$

$$h_{2}(\hat{\mathbf{r}},t) = 2\chi \operatorname{Im} \{E_{X}(\hat{\mathbf{r}},t) E_{Z}^{*}(\hat{\mathbf{r}},t)\}$$

$$h_{3}(\hat{\mathbf{r}},t) = 2\chi \operatorname{Im} \{E_{X}(\hat{\mathbf{r}},t) E_{Y}^{*}(\hat{\mathbf{r}},t)\},$$

$$(2.21)$$

where Im $\{...\}$ is the imaginary part of the quantity in curly brackets and $\chi = A\pi\epsilon_0/4k_0^3\Delta$ (k_0 and A being, respectively, the wavenumber and the Einstein A coefficient for the transition between the upper and lower manifolds, Δ the laser detuning and ϵ_0 the permittivity of free space).

The quantity proportional to $h_0(\hat{\mathbf{r}},t)$ in Eq. (2.16) represents a dynamical effect of the laser fields on the ion which does not cause any effect on its internal degrees of freedom; the term proportional to $h_3(\hat{\mathbf{r}},t)$ represents a A.C. Stark shift of the two internals levels; the terms proportional to $h_1(\hat{\mathbf{r}},t)$ and $h_2(\hat{\mathbf{r}},t)$ represent transitions between the two levels of the lower manifold. If we make the requirement that the lasers are plane-polarized along the axis of quantization Z, then it is clear from the above formulas that $h_1 = h_2 = h_3 = 0$ and only the first term involving h_0 has any effect.

Let us assume that two laser beams, designated the pump (p) and the Stokes (s) beams are present, both plane polarized in the Z-direction, i.e.

$$E_X(\hat{\mathbf{r}},t) = 0,$$

$$E_Y(\hat{\mathbf{r}}, t) = 0,$$

$$E_Z(\hat{\mathbf{r}}, t) = E^{(p)} \exp\left[-i\left(\mathbf{k}_p \cdot \hat{\mathbf{r}} - \omega_p t\right)\right] + E^{(s)} \exp\left[-i\left(\mathbf{k}_s \cdot \hat{\mathbf{r}} - \omega_s t\right)\right]. \quad (2.22)$$

The interaction Hamiltonian in this case is given by

$$\hat{H}_{I} = \chi \left\{ \left| E^{(p)} \right|^{2} + \left| E^{(s)} \right|^{2} + 2 \left| E^{(p)} E^{(s)*} \right| \cos \left[(\mathbf{k}_{p} - \mathbf{k}_{s}) \cdot \hat{\mathbf{r}} - (\omega_{p} - \omega_{s}) t + \phi \right] \right\}, \quad (2.23)$$

where $\phi = \operatorname{Arg}\left\{E^{(p)}E^{(s)*}\right\}$ is the phase difference between the two lasers. The constant terms involving $\left|E^{(p)}\right|^2$ and $\left|E^{(s)}\right|^2$ have no effect on the evolution, and so will be neglected. Thus the full Hamiltonian, including the effect of the harmonic evolution of the ion along the weak axis of the trap (but excluding the internal free evolution) is

$$\hat{H} = \frac{\hat{p}^2}{2m} + \frac{m\omega^2 \hat{x}^2}{2} + \frac{\varepsilon}{k}\cos(k\hat{x} - \Omega t). \tag{2.24}$$

where $\Omega = \omega_p - \omega_s$. The parameters ε and k, which will feature prominently in what follows, are given by

$$\varepsilon = \frac{A\pi\epsilon_0 k}{2k_0^3 \Delta} \left| E^{(p)} E^{(s)*} \right|, \qquad (2.25)$$

$$k = (\mathbf{k}_p - \mathbf{k}_s) \cdot \mathbf{e_x} \tag{2.26}$$

where $\mathbf{e}_{\mathbf{x}}$ is the unit vector along the x-axis, i.e. the axis of weak confinement in the trap.

3 Classical Limit

In the classical limit $(\hat{p} \to p, \hat{x} \to x)$, the Hamiltonian (2.24) takes the form,

$$H = \frac{p^2}{2m} + \frac{m\omega^2 x^2}{2} + \frac{\varepsilon}{k}\cos(kx - \Omega t), \tag{3.1}$$

The classical equations of motion in (p, x) variables are

$$\dot{p} = -\frac{\partial H}{\partial x} = -m\omega^2 x + \varepsilon \sin(kx - \Omega t), \quad \dot{x} = \frac{\partial H}{\partial p} = \frac{p}{m}.$$
 (3.2)

Equations (3.2) lead to the following second order non-linear differential equation,

$$\ddot{x} + \omega^2 x = \frac{\varepsilon}{m} \sin(kx - \Omega t). \tag{3.3}$$

3.1 Dynamics near resonances

Assume that the driving frequency is close to a resonance, i.e.

$$N\omega \approx \Omega,$$
 (3.4)

where N is an integer. In this case, it is convenient to describe a classical dynamics using the "action-angle" variables [20, 21, 22], (I, φ) , which are related to the variables (p, x) by the canonical transformation (see Appendix B),

$$x = \sqrt{\frac{2NI}{\omega m}}\cos\left(\frac{\varphi + \Omega t}{N}\right), \quad p = -\sqrt{2NI\omega m}\sin\left(\frac{\varphi + \Omega t}{N}\right).$$
 (3.5)

In the variables (I, φ) , the Hamiltonian (3.1) takes the form,

$$H = (N\omega - \Omega)I + \frac{\varepsilon}{k}\cos\left(k\sqrt{\frac{2NI}{\omega m}}\cos\Phi - \Omega t\right),\tag{3.6}$$

where

$$\Phi = \frac{\varphi + \Omega t}{N}.\tag{3.7}$$

The second term in (3.6) can be expanded as a series of Bessel functions $J_n(z)$,

$$\cos\left(k\sqrt{\frac{2NI}{\omega m}}\cos\Phi - \Omega t\right) = \sum_{n=-\infty}^{\infty} J_n\left(k\sqrt{\frac{2NI}{m\omega}}\right)\cos[n(\Phi + \pi/2) - \Omega t]. \tag{3.8}$$

We have for the phase, $n(\Phi + \pi/2) - \Omega t$,

$$n(\Phi + \pi/2) - \Omega t = n\frac{\varphi}{N} + \frac{n\pi}{2} + \frac{n-N}{N}\Omega t. \tag{3.9}$$

Thus, the classical Hamiltonian (3.6) can be represented in the form where the unperturbed part and the perturbation are explicitly separated,

$$H = H_0 + H_{int}, (3.10)$$

where

$$H_0 = (N\omega - \Omega)I + \frac{\varepsilon}{k}J_N\left(k\sqrt{\frac{2NI}{m\omega}}\right)\cos(\varphi + N\pi/2), \tag{3.11}$$

$$H_{int} = \frac{\varepsilon}{k} \sum_{n \neq N} J_l \left(k \sqrt{\frac{2NI}{m\omega}} \right) \cos \left(\frac{n}{N} \varphi + \frac{n\pi}{2} + \frac{n-N}{N} \Omega t \right). \tag{3.12}$$

In the (I,φ) variables, the classical equations of motion are,

$$\dot{I} = -\frac{\partial H}{\partial \varphi} = \frac{\varepsilon}{k} J_N(z) \sin(\varphi + \pi N/2) + \tag{3.13}$$

$$\frac{\varepsilon}{kN} \sum_{n \neq N} n J_n(z) \sin\left(\frac{n}{N}\varphi + \frac{n\pi}{2} + \frac{n-N}{N}\right). \tag{3.14}$$

$$\dot{\varphi} = \frac{\partial H}{\partial I} = N\omega - \Omega + \varepsilon \sqrt{\frac{N}{2m\omega I}} J_N'(z) \cos(\varphi + \pi N/2) + \tag{3.15}$$

$$\varepsilon \sqrt{\frac{N}{2m\omega I}} \sum_{n \neq N} J_l'(z) \cos\left(\frac{n}{N}\varphi + \frac{n\pi}{2} + \frac{n-N}{N}\right),$$
 (3.16)

where,

$$z = k\sqrt{\frac{2NI}{m\omega}},\tag{3.17}$$

is a dimensionless variable. Equations (3.14) and (3.16) are convenient when analyzing the classical dynamics in the vicinity of the resonance (3.4). This case corresponds to small values of ε ,

$$\varepsilon < \varepsilon_{cr}.$$
 (3.18)

Usually, the critical parameter ε_c in (3.18) should be found numerically (see Sec. 5). Under the condition (3.18), classical dynamics can be approximately described by the Hamiltonian H_0 (3.11). The corresponding approximate equations of motion follow from Eqs (3.14) and (3.16),

$$\dot{I} = -\frac{\partial H}{\partial \varphi} = \frac{\varepsilon}{k} J_N(z) \sin(\varphi + \pi N/2),$$
 (3.19)

$$\dot{\varphi} = \frac{\partial H}{\partial I} = N\omega - \Omega + \varepsilon \sqrt{\frac{N}{2m\omega I}} J_N'(z) \cos(\varphi + \pi N/2). \tag{3.20}$$

In the general case (for ε large), it is more convenient to use the following exact equations written in (I, φ) variables,

$$\dot{I} = -\frac{\varepsilon}{N} \sqrt{\frac{2NI}{m\omega}} \sin\left[k\sqrt{\frac{2NI}{m\omega}} \cos\left(\frac{\varphi + \Omega t}{N}\right) - \Omega t\right] \sin\left(\frac{\varphi + \Omega t}{N}\right), \tag{3.21}$$

$$\dot{\varphi} = N\omega - \Omega - \varepsilon \sqrt{\frac{N}{2m\omega I}} \sin \left[k \sqrt{\frac{2NI}{m\omega}} \cos \left(\frac{\varphi + \Omega t}{N} \right) - \Omega t \right] \cos \left(\frac{\varphi + \Omega t}{N} \right) (3.22)$$

3.2 Dimensionless variables

To describe both the classical and quantum dynamics, it is convenient to introduce the following dimensionless variables,

$$\tau = \omega t, \qquad \xi = kx, \qquad \ell = \frac{I}{\hbar},$$

$$\mathcal{H}_0 = \frac{H_0}{\hbar \omega}, \quad \mathcal{H}_{int} = \frac{H_{int}}{\hbar \omega}, \quad \mathcal{H} = \frac{H}{\hbar \omega},$$
(3.23)

and the dimensionless parameters,

$$\epsilon = \frac{\varepsilon k}{m\omega^2}, \quad \eta^2 = \frac{\hbar k^2}{2m\omega}, \quad \mu = \frac{\Omega}{\omega}, \quad \delta = N - \mu.$$
(3.24)

The parameter η is the Lamb-Dicke parameter used in the theory of ion traps to quantify the strength of confinement. It is related to effective Planck constant by the formula $\bar{h} = 2\eta^2$.

3.3 Isolated Nonlinear Resonance

Using (3.23) and (3.24), we have from (3.19) and (3.20) the approximate dimensionless equations of motion in the vicinity of the resonance (3.4),

$$\frac{d\ell}{d\tau} = -\frac{\partial \mathcal{H}_0}{\partial \varphi} = \frac{\epsilon}{2\eta^2} J_N(z) \sin(\varphi + \pi N/2), \qquad (3.25)$$

$$\frac{d\varphi}{d\tau} = \frac{\partial \mathcal{H}_0}{\partial \ell} = \delta + \frac{\epsilon}{2\eta} \sqrt{\frac{N}{\ell}} J_N'(z) \cos(\varphi + \pi N/2), \tag{3.26}$$

where $z = 2\eta\sqrt{N\ell}$ and the dimensionless resonant Hamiltonian is,

$$\mathcal{H}_0 = \ell \delta + \frac{\epsilon}{2\eta^2} J_N(z) \cos(\varphi + \pi N/2). \tag{3.27}$$

The classical dynamics corresponding the Hamiltonian (3.27) we shall call "Nonlinear Resonance" (NR).

To estimate the region of parameters of validity of Eqs (3.25) and (3.26), their solutions should be compared with the solutions of exact equations (3.21) and (3.22). Equations (3.21) and (3.22) in the dimensionless variables have the form,

$$\frac{d\ell}{d\tau} = -\frac{\epsilon}{\eta} \sqrt{\frac{\ell}{N}} \sin\left[z\cos\left(\frac{\varphi + \mu\tau}{N}\right) - \mu\tau\right] \sin\left(\frac{\varphi + \mu\tau}{N}\right), \tag{3.28}$$

$$\frac{d\varphi}{d\tau} = \delta - \frac{\epsilon}{2\eta} \sqrt{\frac{N}{\ell}} \sin\left[z\cos\left(\frac{\varphi + \mu\tau}{N}\right) - \mu\tau\right] \cos\left(\frac{\varphi + \mu\tau}{N}\right). \tag{3.29}$$

Equations (3.28) and (3.29) are derived from the exact dimensionless Hamiltonian,

$$\mathcal{H} = \ell \delta + \frac{\epsilon}{2\eta^2} \cos \left[z \cos \left(\frac{\varphi + \mu \tau}{N} \right) - \mu \tau \right]. \tag{3.30}$$

In the dimensionless variables (3.23) and (3.24), Eq. (3.3) takes the form,

$$\frac{d^2\xi}{d\tau^2} + \xi = \epsilon \sin(\xi - \mu\tau). \tag{3.31}$$

4 Quantum Equations of Motion

In the dimensionless notation (3.23) and (3.24), the quantum Hamiltonian (2.24) takes the following form in the coordinate representation,

$$\frac{\hat{H}}{\hbar\omega} = \mathcal{H} = \frac{1}{2\eta^2} \left[-2\eta^4 \frac{\partial^2}{\partial \xi^2} + \frac{\xi^2}{2} + \epsilon \cos(\xi - \mu \tau) \right]. \tag{4.1}$$

The Schrödinger equation for the Hamiltonian (4.1) is,

$$i2\eta^2 \frac{\partial \Psi(\xi, \tau)}{\partial \tau} = \left[\hat{\mathcal{H}}_{LO} + \epsilon \cos(\xi - \mu \tau) \right] \Psi(\xi, \tau), \tag{4.2}$$

where $\hat{\mathcal{H}}_{LO}$ is the Hamiltonian of a linear oscillator,

$$\hat{\mathcal{H}}_{LO} = -2\eta^4 \frac{\partial^2}{\partial \xi^2} + \frac{\xi^2}{2}.\tag{4.3}$$

For h_0 we have the well-known eigenvalue problem,

$$\hat{\mathcal{H}}_{LO}|n\rangle = 2\eta^2(n+1/2)|n\rangle,\tag{4.4}$$

where,

$$|n\rangle \equiv \phi_n(\xi) = \left[\frac{1}{\eta 2^n n! \sqrt{2\pi}}\right]^{1/2} H_n(\xi/\sqrt{2\eta}) e^{-\xi^2/4\eta^2},$$
 (4.5)

where $H_n(y)$ is a Hermite polynomial. Although these eigenfunction may appear somewhat unfamiliar because of the use of dimensionless variables, they are in fact the standard eigenfunctions of an unperturbed harmonic oscillator (i.e. the Hamiltonian given by Eq. (2.1) with $\hat{H}_I = 0$). The normalization condition for the eigenfunction $\phi_n(\xi)$ is,

$$\int_{-\infty}^{\infty} \phi_n(\xi)\phi_m(\xi)d\xi = \delta_{n,m}.$$
(4.6)

To describe the quantum dynamics we represent the wave function in (4.2) in the form,

$$\Psi(\xi,\tau) = \sum_{n=0}^{\infty} c_n(\tau)\phi_n(\xi). \tag{4.7}$$

From (4.2) we have the equations for the complex amplitudes, $c_n(\tau)$,

$$i\frac{dc_{m}(\tau)}{d\tau} = (m+1/2)c_{m}(\tau) + \frac{\epsilon}{2\eta^{2}} \sum_{n=0}^{\infty} \langle m | \cos(\xi - \mu \tau) | n \rangle c_{n}(\tau)$$

$$= (m+1/2)c_{m}(\tau) + \frac{\epsilon}{4\eta^{2}} \sum_{n=0}^{\infty} \left(e^{-i\mu\tau} F_{m,n}(\eta) + e^{i\mu\tau} F_{m,n}^{*}(\eta) \right) c_{n}(\tau). (4.8)$$

In Eqs (4.8), $F_{m,n}(\eta)$ is the matrix element,

$$F_{m,n}(\eta) = \langle m|e^{i\xi}|n\rangle = \frac{1}{\sqrt{\pi 2^{m+n}m!n!}} \int_{-\infty}^{\infty} H_m(u)H_n(u)e^{-u^2+i2\eta u}du.$$
 (4.9)

Equations (4.8) are used below, in Sec. 5, for numerical calculation of the quantum dynamics of the system.

5 Results of Numerical Calculations

In this section, we present results of numerical simulations of classical and quantum dynamics of systems whose Hamiltonians have the form given by Eq. (2.24). We have used a set of parameters which will allow easy experimental verification of our predictions using the type of ion trap apparatus currently being used to investigate quantum computation.

If we use the geometry for the pump and Stokes lasers shown in Fig.1, the parameter k defined by Eq. (2.26) is given by $k = \cos \theta(k_p + k_s) \approx 2k_0 \cos \theta$. The laser field strengths $|E^{(p)}|$ and $|E^{(s)}|$ can be related to the power in the pump and the Stokes beams respectively. It is usual to generate one of these beams (the Stokes, say) by frequency modulation of the pump beam, so that the beam parameters will be similar for them both. The power in the pump beam is given by the formula (Ref. [35], p. 488)

$$P = \frac{c\epsilon_0 \pi}{4} w_0^2 \left| E^{(p)} \right|^2 \tag{5.10}$$

where w_0 is the laser spot size (i.e. the $1/e^2$ radius of the intensity distribution). If we substitute this result into Eq. (2.25), we obtain the following expression for the dimensionless parameter ϵ :

$$\epsilon = \frac{\varepsilon k}{m\omega^2}$$

$$= \frac{8A\theta P}{ck_0 m\omega^2 w_0^2 \Delta} s \cos^2, \tag{5.11}$$

where $s = \left| E^{(s)} \right| / \left| E^{(p)} \right|$ is a dimensionless parameter of order unity which can be controlled experimentally.

Singly ionized calcium $(m=6.64\times 10^{-26} {\rm kg})$ is common ion in use by several groups worldwide for ion-trap quantum research (see Fig. 3, for energy levels of this ion). For the ${}^2S_{1/2}-{}^2P_{1/2}$ transition in this ion (wavelength $\lambda_0=397{\rm nm}$) the Einstein A coefficient is [33] $A=1.30\times 10^8{\rm s}^{-1}$ and the wavenumber is $k_0=2\pi/\lambda_0=1.58\times 10^7{\rm m}^{-1}$. If we assume a laser power of 10mW, a spot size $w_0=20\mu{\rm m}$ a trapping frequency $\omega=2\pi\times 500{\rm kHz}$, and a detuning $\Delta=2\pi\times 1.0{\rm GHz}$, then $\epsilon=1333s\cos^2\theta$. Thus by varying the experimental free parameters s and θ one can achieve a large dynamic range for the dimensionless driving force ϵ . The Lamb-Dicke parameter η for these parameters is $0.502\cos\theta$.

The driving frequency Ω is the difference between the pump and the Stokes frequencies. As mentioned above, these two beams will be realized by splitting one parent beam using a beam splitter and then frequency modulating one of the resultant beam using either an acousto-optic or an electro-optic modulator. In this manner splittings as high as $\Omega = 2\pi \times 100 \mathrm{MHz}$ can be achieved without too much difficulty, so that the dimensionless parameter N can be in the range 0 to 200.

5.1 Simulation of classical dynamics

In Figs 4a and 4b, the classical phase space (Poincare section) is shown in $(\xi, d\xi/d\tau)$ plane, for seven initial conditions, and for different values of the dimensionless driving force, ϵ , which characterizes the intensity of the laser beams, and is defined in (5.11). To derive these results, the Eq. (3.31) was solved numerically (for N=4 and $\delta=10^{-2}$). One can see from Fig. 4a, that for small values of ϵ ($\epsilon < 2$) the classical dynamics is regular in some regions of the phase space. Note, that even at these values of ϵ there exist relatively large regions in the phase space with the chaotic component. When the interaction parameter ϵ increases, the regions with the regular classical dynamics become smaller. As one can see from Fig. 4a, even at $\epsilon = 4$, the dynamics in the region of the phase space corresponding to the "classical ground state" (CGS) (the vicinity of the point (0,0)) remains regular. At larger values of ϵ ($\epsilon \approx 8$) the CGS becomes chaotic. This transition is demonstrated in Fig. 4b. Figs 5 and 6, show the time evolution of the dimensionless classical coordinate of the ion, $\xi(\tau)$. The maximum dimensionless time of simulations, $\tau_{max}=100$, corresponds to the real time-scale $t_{max}=31.8\mu s$

 $(\omega = 2\pi \times 500 \mathrm{kHz})$. The initial conditions for the dynamics shown in Figs 5 and 6 correspond to the CGS. As one can see from Fig. 5, the chaotic component appears at $\epsilon \approx 8$, and is well resolved for $\epsilon > 10$ (see Fig. 6). The frequency Fourier transform for the dynamics shown in Figs 5 and 6, is presented in Figs 7 and 8. It is well-known, that the transition to the dynamical chaos in classical dynamical systems is accompanied by the transition in the frequency Fourier spectrum. The regular dynamics corresponds to the discrete frequency spectrum, the chaotic dynamics corresponds to the continuous frequency spectrum. This characteristic modification of the frequency spectrum is demonstrated in Figs 7 and 8. For small values of the dimensionless driving force ϵ , one can see only some quasi-discrete lines in the Fourier spectrum. When ϵ increases, the frequency spectrum transforms to the continuous one.

5.2 Simulation of quantum dynamics

To simulate a quantum dynamics the following parameters were chosen: N=4, $\delta = 10^{-2}$, $\eta = 0.45$. For the initial conditions we used the ground state of the unperturbed quantum linear oscillator: $c_0(0) = 1$, $c_n(0) = 0$ for n > 0. Fig. 9, shows the time evolution of the quantum probabilities $P_n(\tau) \equiv |c_n(\tau)|^2$ (n=0, 1, 2, 3, 4 and 5) for relatively small values of $\epsilon = 0, 0.5, 1, 1.5$ and 2. These values of ϵ correspond to the regular classical dynamics which starts from the CGS. Time evolution of quantum probabilities $P_n(\tau)$ (n = 0, 1, 2 and 3) for bigger values of ϵ is shown in Fig. 10. Because the value of the parameter $\epsilon \approx 8$ corresponds to the classical chaotic dynamics for the initially populated CGS, the curves (4) in Fig. 10 describe the quantum chaotic motion. Fig. 11, shows the dynamics of the probability function $P_0(\tau)$ for the larger time interval: $\tau \in [0,30]$. In the real time this correspond to: $t \in [0,9.54]\mu s$. As one can see from Fig. 11, for $\epsilon > 7.5$ the dynamics of the probability function $P_0(\tau)$ becomes rather complicated, and correspond to the classical chaotic motion. We hope that this complicated dynamics of the probability functions $P_n(\tau)$ can be measured directly in the experiments with trapped ion. Fig. 12, represents the results of the numerical simulations of the frequency Fourier spectrum, $P_0(\nu)$, of the quantum probability function $P_0(\tau)$. As one can see from Fig. 12, the characteristic qualitative modification of the frequency spectrum $P_0(\nu)$ starts from $\epsilon > 7.5$. This modification of the frequency Fourier spectrum can also be measured experimentally. In Fig. 13, we show the results of numerical simulation of the dynamical evolution of the average value: $\langle \xi^2 \rangle \equiv \langle \Psi(\xi, \tau) | \xi^2 | \Psi(\xi, \tau) \rangle$, where the wave function $\Psi(\xi, \tau)$ is defined in (4.7). This dynamical characteristic is very important for understanding the conditions of stability of the system under consideration, as it describes the amplitude of the ion's oscillations in a trap due to the influence of the resonant laser fields. Experimental measuring the time dependence of this amplitude is important for characterizing the regular and chaotic dynamics of an ion. The frequency spectrum of the amplitude $\langle \xi^2 \rangle$ is shown in Fig. 14 for different values of the perturbation parameter ϵ . As one can see from Fig. 14, at $\epsilon > 7.5$, the frequency spectrum qualitatively modifies, and includes many harmonics. In Fig. 15, we show the time evolution of two functions: the unperturbed Hamiltonian of quantum linear oscillator (4.3), $\langle \hat{\mathcal{H}}_{LO} \rangle$, and the amplitude $\langle \xi^2 \rangle$, for the values of the perturbation parameter $\epsilon = 0; 05; 2$. The corresponding classical dynamics is regular in this case. The time evolution of the same functions is shown in Fig. 16 for larger values of the parameter $\epsilon = 3; 5; 7.5; 8$. The curves (3) and (4) correspond to the classically chaotic regime of motion. The maximum simulation time at Fig. 16 is: $t_{max} = 4.77\mu$ s.

6 Conclusion

In this paper, we introduced a quantum model which describes a transition from a regular dynamics to quantum chaos, for a single ion in a linear ion trap. The configuration of the resonant laser fields allowed us to represent the model in a "standard" form. Namely, our model formally describes a quantum linear oscillator interacting with a one-dimensional plane wave (see the Hamiltonian (2.29)). The classical version of this model is very important and useful in the theory of the dynamical chaos [9]. This model differs significantly from the "usual" nonlinear models (as, for example, a "standard map" [8, 10]) considered in the theoretical works on dynamical chaos. Namely, the model described by the Hamiltonian (2.19) includes "nonlinearity" and "perturbation" in the same term. In this sense, this model is degenerated, and possesses many unusual properties [9]. So, quantum analysis of this model both theoretically and experimentally will be of significant importance for understanding complicated dynamics in this system, and for applications in different devices based on the trapped ions, including quantum computer. The numerical results presented in this paper describe both regular and chaotic quantum dynamics which starts from the initial population of the linear oscillator's ground state. We believe that this regime of motion should be investigated in the experiments with the trapped single ion. These experiments will allow one to establish qualitative and quantitative correspondence between the quantum dynamics described by the Hamiltonian (2.29) and the real system "a single trapped ion + resonant laser fields". Further theoretical analysis and experiments should include both pure quantum and quasiclassical regions of initial population, and the parameters describing regular and chaotic regimes in both these regions. These investigations are now in progress.

Acknowledgments

It is a pleasure to thank G.D. Doolen, G. Milburn, and J. Rehacek for valuable discussions. This work was partly supported by the National Security Agency, and by the Department of Energy under contract W-7405-ENG-36.

Appendix A: Derivation of Eq. (2.21)

The dipole matrix elements appearing in Eq. (2.11) can be written in terms of the Einstein A coefficient between the upper and lower manifolds as follows:

$$\langle \mu | \hat{d}_i | \lambda \rangle = \sqrt{\frac{3Ac^2 (2J_{\lambda} + 1)}{4\omega_0^2 \alpha}} \sum_{q=-1}^{1} \begin{pmatrix} J_{\mu} & 1 & J_{\lambda} \\ -m_{\mu} & q & m_{\lambda} \end{pmatrix} e_i^{(q)}$$
 (A.1)

where c is the speed of light, α is the fine structure constant, ω_0 is the angular frequency of the transition between the upper and lower manifolds, $(J_{\lambda}, m_{\lambda})$ are the magnetic quantum numbers for the upper manifold state $|\lambda\rangle$ (J_{μ}, m_{μ}) are the magnetic quantum numbers for the lower manifold state $|\mu\rangle$, the term contain six quantities in brackets is the Wigner 3-j symbol, and $e_i^{(q)}$ is the *i*-th component of the *q*-th normalized spherical basis vector, viz.

$$\mathbf{e}^{(1)} = -\frac{1}{\sqrt{2}}(1, -i, 0),$$
 (A.2)

$$\mathbf{e}^{(0)} = (0, 0, 1), \tag{A.3}$$

$$\mathbf{e}^{(-1)} = \frac{1}{\sqrt{2}}(1, i, 0).$$
 (A.4)

(A.5)

Substituting Eq. (A.1) into Eq. (2.11), and assuming that the Zeeman splitting in the upper manifold is small compared to the overall detuning, so that $\Delta_{\lambda} \approx \Delta$ (independent of λ), then we find that the quantities $\langle \mu, \nu \rangle$ are given by the following formula:

$$\kappa_{\mu,\nu}\left(\hat{\mathbf{r}},t\right) = \frac{3\pi\epsilon_0 A c^3}{4\omega_0^3 \Delta} \Lambda_{ij}\left(\mu,\nu\right) E_i\left(\hat{\mathbf{r}},t\right) E_j^*\left(\hat{\mathbf{r}},t\right), \tag{A.6}$$

where the tensor $\Lambda_{ij}(\mu,\nu)$ is given by

$$\Lambda_{ij}(\mu,\nu) = (2J_{\lambda} + 1) \sum_{m_{\lambda} = -J_{\lambda}}^{J_{\lambda}} \sum_{q,q' = -1}^{1} \begin{pmatrix} J_{\mu} & 1 & J_{\lambda} \\ -m_{\mu} & q & m_{\lambda} \end{pmatrix} \begin{pmatrix} J_{\nu} & 1 & J_{\lambda} \\ -m_{\nu} & q' & m_{\lambda} \end{pmatrix} e_{i}^{(q)} e_{j}^{(q')*}$$
(A.7)

If we assume that the lower manifold is the ${}^2S_{1/2}$ ground state of an alkali ion, the two states being denoted $|1\rangle = {}^2S_{1/2}, m = -1/2$ and $|2\rangle = {}^2S_{1/2}, m = 1/2$, and that the upper manifold is the ${}^2P_{1/2}$ state, then these tensors can be found in closed form:

$$\Lambda_{ij}(1,1) = \Lambda_{ij}^{*}(2,2) = \frac{1}{3} \begin{pmatrix} 1 & -i & 0 \\ i & 1 & 0 \\ 0 & 0 & 1 \end{pmatrix},$$

$$\Lambda_{ij}(1,2) = -\Lambda_{ij}^{*}(2,1) = \frac{1}{3} \begin{pmatrix} 0 & 0 & -1 \\ 0 & 0 & -i \\ 1 & i & 0 \end{pmatrix}.$$
(A.8)

Therefore the cross products involving the electric field components with these tensors can be written as follows:

$$\Lambda_{ij}(1,1) E_i E_j^* = \frac{1}{3} \left[|\mathbf{E}|^2 + 2 \text{Im} \left\{ E_X E_Y^* \right\} \right], \tag{A.9}$$

$$\Lambda_{ij}(2,2) E_i E_j^* = \frac{1}{3} \left[|\mathbf{E}|^2 - 2 \text{Im} \left\{ E_X E_Y^* \right\} \right],$$
 (A.10)

$$\Lambda_{ij}(1,2) E_i E_j^* = \frac{1}{3} [E_Z (E_X^* + i E_Y^*) - E_Z^* (E_X + i E_Y)], \qquad (A.11)$$

$$\Lambda_{ij}(2,1) E_i E_j^* = \frac{1}{3} \left[-E_Z \left(E_X^* - i E_Y^* \right) + E_Z^* \left(E_X - i E_Y \right) \right]. \tag{A.12}$$

If these results are substituted into the definition of h_0 and h_i , Eqs (2.17)-(2.20), one obtains Eq. (2.21). Similar results, with slightly different numerical factors, are obtained if the upper manifold is a ${}^2P_{3/2}$ state.

Appendix B: Canonical Transform to "action-angle" variables

The theory of canonical transforms in classical mechanics is described in detail in Ref. [36], §45. We want to transform from a set of variable x, p to a new set φ, I , where φ plays the role of position coordinate and I the role of momentum. Such transforms are specified by a *generating function*, $F(x, \varphi, t)$. Then variables p and I and the Hamiltonian in the new coordinate system are are related to F by the following

formulas:

$$p = \frac{\partial F}{\partial x},\tag{B.1}$$

$$I = -\frac{\partial F}{\partial \varphi}, \tag{B.2}$$

$$H(\varphi, I) = H(x, p) + \frac{\partial F}{\partial t}$$
 (B.3)

For the canonical transform used in section 3.1, the generating function is given by

$$F(x,\varphi,t) = -\frac{m\omega}{2}x^2 \tan\left(\frac{\varphi + \Omega t}{N}\right). \tag{B.4}$$

Substituting, we find:

$$p = -m\omega x \tan\left(\frac{\varphi + \Omega t}{N}\right) \tag{B.5}$$

$$I = -\frac{m\omega}{2N}x^2\sec^2\left(\frac{\varphi + \Omega t}{N}\right)$$
 (B.6)

$$H(\varphi, I) = H(x, p) - \frac{m\omega\Omega}{2N}x^2\sec^2\left(\frac{\varphi + Omegat}{N}\right)$$
 (B.7)

$$= H(x,p) - \Omega I. \tag{B.8}$$

Equation (B.5) implies that

$$x = \sqrt{\frac{2NI}{m\omega}}\cos\left(\frac{\varphi + \Omega t}{N}\right). \tag{B.9}$$

On substitution of this last formula into Eq. (B.6) we obtain

$$p = -\sqrt{2Nm\omega I}\sin\left(\frac{\varphi + \Omega t}{N}\right). \tag{B.10}$$

References

- [1] R.J. Hughes, D.F.V. James, J.J. Gomez, M.S. Gulley, M.H. Holzscheiter, P.G. Kwiat, S.K. Lamoreaux, C.G. Peterson, V. D. Sandberg, M.M. Schauer, C.M. Simmons, C.E. Thorburn, D. Tupa, P.Z. Wang and A.G. White, "The Los Alamos Trapped Ion Experiment", Fortschritte der Physik, 46, 329 (1998).
- [2] G.P. Berman, G.D. Doolen, R. Mainieri and V.I. Tsifrinovich, *Introduction to Quantum Computers*, World Scientific, Singapore, 1998.
- [3] G.P. Berman and G.M. Zaslavsky, "Condition of Stochasticity in Quantum Non-linear Systems", *Physica A*, **91**, 450 (1978).
- [4] G.P. Berman and G.M. Zaslavsky, "Logarithm Breaking Time in Quantum Chaos", In: *Quantum Chaos*, G. Casati, B. Chirikov (Eds), Cambridge University Press, 1995, p. 435.
- [5] G.P. Berman, E.N. Bulgakov, D.D. Holm, "Crossover-Time in Quantum Boson and Spin Systems", Springer-Verlag, 1994.
- [6] G.P. Berman, G.M. Zaslavsky, "Theory of Quantum Nonlinear Resonance", Phys. Lett. A, 61, 295 (1977).
- [7] B.V. Chirikov, "Research Concerning the Theory of Nonlinear Resonance and Stochasticity", *CERN Tran.*, 71-40, Geneva.
- [8] B.V. Chirikov, *Phys. Reports*, **52**, 263 (1979).
- [9] G.M. Zaslavsky, Chaos in Dynamic Systems, Harwood Academic Publ., NY, 1985.
- [10] A. Lichtenberg, M. Lieberman, Regular and Chaotic Motion, Springer, 1983.
- [11] G.P. Berman, G.M. Zaslavsky, A.R. Kolovsky, "Interaction of Quantum Nonlinear Resonances", Sov. Phys. JETP, **54**, 272 (1981).
- [12] G.P. Berman, A.R. Kolovsky, "Quantum Chaos in Interactions of Multilevel Quantum Systems With Coherent Radiation Field", Sov. Phys. Usp., 35, 303 (1992).
- [13] G.P. Berman, O.F. Vlasova, F.M. Izrailev, "Quasienergy Functions and Spectrum of Two Interacting Nonlinear Resonances in the Region of Classical Chaos", *Sov. Phys. JETP*, **66**, 269 (1987).

- [14] G.P. Berman, A.R. Kolovsky, "Quantum Chaos in Diatomic Molecule Interacting With a Resonant Field", Sov. Phys. JETP, 68, 818 (1989).
- [15] G.P. Berman, E.N. Bulgakov, D.D. Holm, "Nonlinear Resonance and Dynamical Chaos in a Diatomic Molecule Driven by a Resonant IR Field", *Phys. Rev. A*, 52, 3074 (1995).
- [16] G.P. Berman, E.N. Bulgakov, D.K. Campbell, I.V. Krive, "Quantum nonlinear resonance and quantum chaos in Aharonov-Bohm oscillations", *Phys. Rev. B*, 56, 10338 (1997).
- [17] G.P. Berman, A.R. Kolovsky, "Renormalization Method for the Quantum System of Interacting Resonances", *Phys. Lett. A*, **125**, 188 (1987).
- [18] L.E. Reichl, "The Transition to Chaos in Conservative Classical Systems: Quantum Manifestations", Springer-Verlag, 1992.
- [19] J.E. Bayfield, S.Y. Luie, L.C. Perotti, M.P. Skrzypkowski, "Ionization Steps and Phase-Space Metamorphoses in the Pulsed Microwave Ionization of Highly Excited Hydrogen Atoms", *Phys. Rev. A*, **53**, R12 (1996).
- [20] G.M. Zaslavsky, R.Z. Sagdeev, D.A. Usikov, A.A. Chernikov, Weak Chaos and Quasi-Regular Patterns, Cambridge University Press, 1992.
- [21] A.A. Chernikov, R.Z. Sagdeev, D.A. Usikov, M.Yu. Zakharov and G.M. Zaslavsky, "Minimal Chaos and Stochastic Webs", *Nature*, **326**, 559 (1987).
- [22] A.A. Chernikov, M.Ya. Natenzon, B.A. Petrovichev, R.Z. Sagdeev and G.M. Zaslavsky, "Strong Changing of Adiabatic Invariants, KAM-Tori and Web-Tori", Phys. Lett. A, 129, 377 (1998).
- [23] J.K. Breslin, C.A. Holmes, G.J. Milburn, "Quantum Signatures of Chaos in the Dynamics of a Trapped Ion", *Phys. Rev. A*, **56**, 3022 (1997).
- [24] G.P. Berman, V.Yu. Rubaev, G.M. Zaslavsky, "The Problem of Quantum Chaos in Kicked Harmonic Oscillator", *Nonlinearity*, 4, 543 (1991).
- [25] M. Frasca, "Quantum Kicked Dynamics and Classical Diffusion", *Phys. Lett. A*, **231**, 344 (1997).

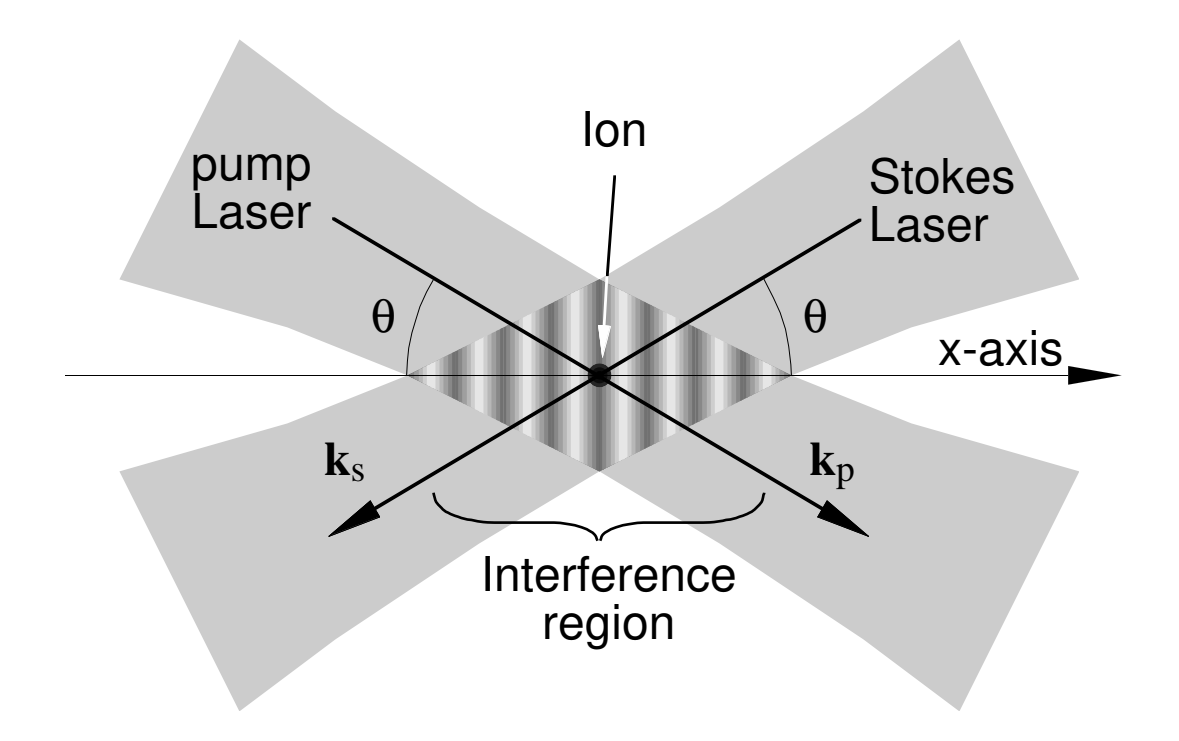
- [26] S.A. Gardiner, J.I. Cirac, P. Zoller, "Quantum Chaos in an Ion Trap: The Delta-Kicked Harmonic Oscillator", Phys. Rev. Lett., 79, 4790 (1997).
- [27] B.G. Klappauf, W.H. Oskay, D.A. Steck, M.G. Raizen, "Observation of Noise and Dissipation Effects on Dynamical Localization", *Phys. Rev. Lett.*, **81**, 1203 (1998).
- [28] B.G. Klappauf, W.H. Oskay, D.A. Steck, M.G. Raizen, "Experimental Study of Quantum Dynamics in a Regime of Classical Anomalous Diffusion", *Phys. Rev. Lett.*, 81, 4044 (1998).
- [29] C. Monroe, D.M. Meekhof, B.E. King and D. J. Wineland "A Schrödinger Cat Superposition State of an Atom", Science, 272, 1131 (1996).
- [30] D.J. Wineland, C. Monroe, D.M. Meekhof, B.E. King, D. Leibfried, W.M. Itano, J.C. Bergquist, D. Berkeland, J.J. Bollinger and J. Miller, "Quantum State Manipulation of Trapped Atomic Ions", Proc. Roy. Soc. (London) A, 454, 411 (1998).
- [31] M. Roberts, P. Taylor, G.P. Barwood, P. Gill, H.A. Klein and W.R.C. Rowley, "Observation of an Electric Octupole Transition in a Single Ion", *Phys. Rev. Lett.*, 78, 1876 (1997);
 D.J. Berkeland, J.D. Miller, J.C. Bergquist, W.M. Itano and D.J. Wineland, "Laser-Cooled Mercury Ion Frequency Standard", *Phys. Rev. Lett.*, 80, 2089 (1998).
- [32] J.I. Cirac and P. Zoller, "Quantum Computation With Cold Trapped Ions", Phys. Rev. Lett., 74, 4091 (1995);
 C. Monroe, D.M. Meekhof, B.E. King, W.M. Itano and D.J. Wineland, "Demonstration of a Fundamental Quantum Logic Gate", Phys. Rev. Lett., 75, 4714 (1995).
- [33] D.F.V. James, "Quantum Dynamics of Cold Trapped Ions with Application to Quantum Computation", Appl. Phys. B, 66, 181 (1998).
- [34] M.S. Gulley, A.G. White and D.F.V. James, "A Method for Performing Quantum Logic Using Stimulated Raman Transitions of Trapped Calcium Ions", to be submitted, 1998.
- [35] P. W. Milonni and J. H. Eberly Lasers (Wiley, New York, 1988).
- [36] L. D. Landau and E. M. Lifshitz, Mechanics, (Pergamon, Oxford, 1960).

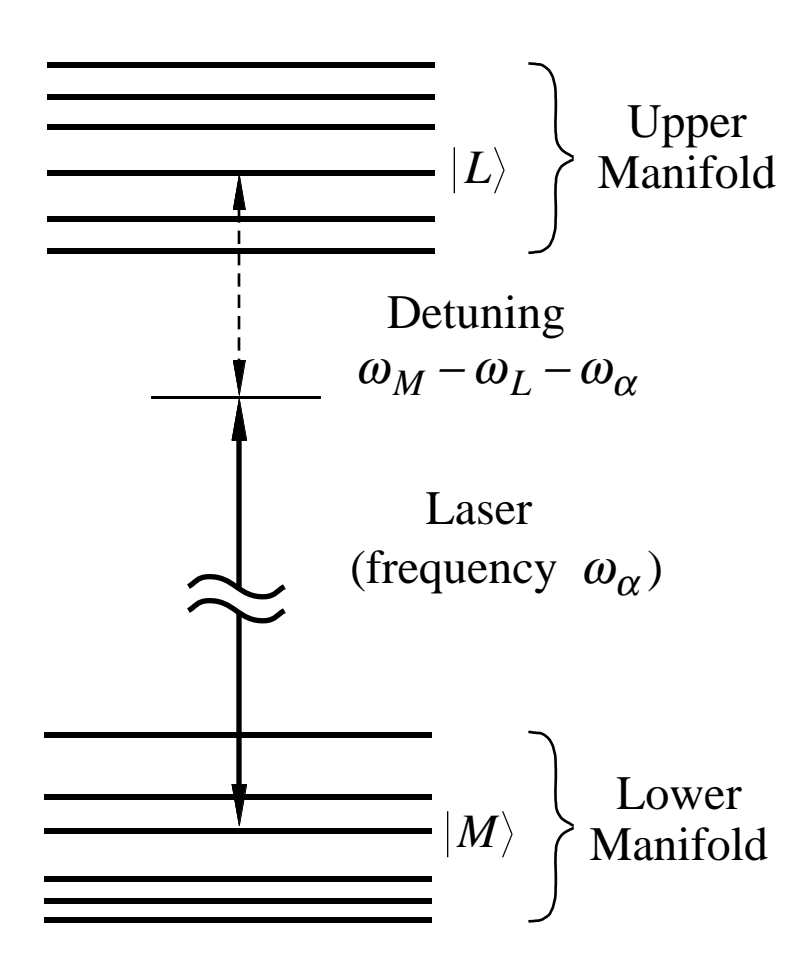
Figure captions

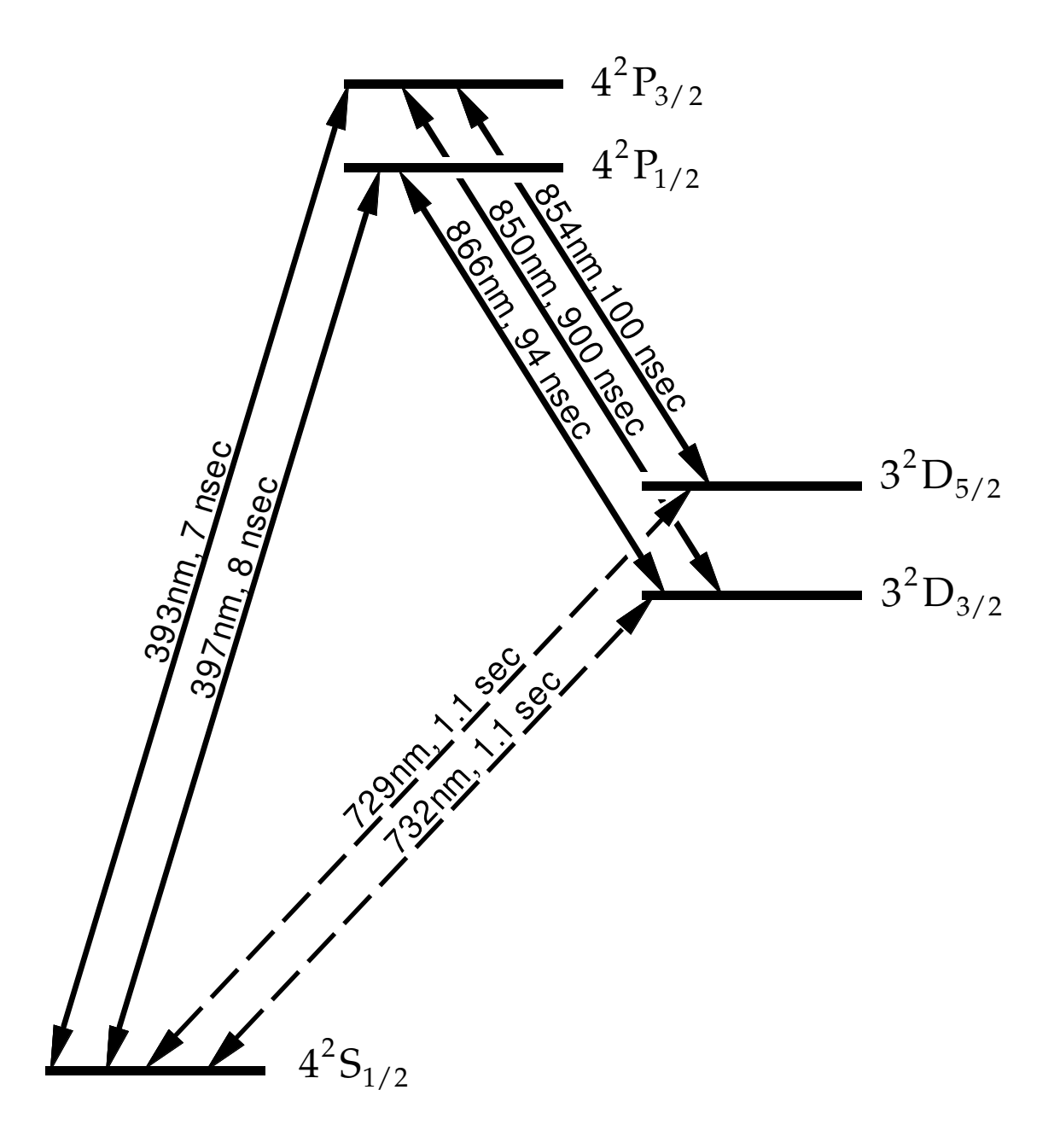
- **Fig. 1:** A schematic diagram of an ion in a linear trap to illustrate the notation and configurations of the laser fields.
- Fig. 2: A schematic illustration of the energy levels of a trapped ion.
- **Fig. 3:** Energy levels of Ca⁺ ion. Wavelengths and radiative lifetimes are shown. See [33] for references.
- **Fig. 4:** Classical phase space (Poincare section). Trajectories with different initial conditions are shown. The values of ϵ are indicated in the figure: (a) $\epsilon = 2, 2.5, 3, 4$; (b) $\epsilon = 5, 8, 10, 20$; $\eta = 0.45$; N = 4, $\delta = 10^{-2}$.
- Fig. 5: Time evolution of the dimensionless classical amplitude of oscillations $\xi(\tau)$ for different values of $\epsilon = 0, 0.5, 1, 2, 5, 8$. The maximum time of simulation it $t_{max} = 31.8\mu$ s. Initial condition: $(\xi, d\xi/d\tau) = (0, 0)$.
- Fig. 6: Chaotic dynamics of the dimensionless classical amplitude of oscillations $\xi(\tau)$ for the values of $\epsilon = 10, 20, 30, 40$. The maximum time of simulation it $t_{max} = 31.8\mu$ s. Initial condition: $(\xi, d\xi/d\tau) = (0, 0)$.
- Fig. 7: Frequency Fourier spectrum of the classical amplitude $\xi(\tau)$ for $\epsilon = 0,0.5,1,2,5$ and 8. Transition to chaos appears at $\epsilon \approx 8$. Initial condition: $(\xi, d\xi/d\tau) = (0,0)$.
- **Fig. 8:** Frequency Fourier spectrum of the chaotic dynamics of the classical amplitude $\xi(\tau)$ for $\epsilon = 10,20,30$ and 40. Transition to chaos appears at $\epsilon \approx 8$. Initial condition: $(\xi, d\xi/d\tau) = (0,0)$.
- Fig. 9: Dynamics of the quantum probabilities: $P_n(\tau) = |c_n(\tau)|^2$, for n = 0,1,2,3,4 and 5, and for $\epsilon = 0, 0.5, 1, 1.5$ and 2. Initial condition: $c_0(0) = 1, c_n(0) = 0$ for (n > 0).
- Fig. 10: Dynamics of the quantum probabilities: $P_n(\tau) = |c_n(\tau)|^2$, for n = 0, 1, 2 and 3, and for $\epsilon = 3, 5$ and 7.5. Initial condition: $c_0(0) = 1$, $c_n(0) = 0$ for (n > 0).
- Fig. 11: Dynamics of the quantum probability: $P_0(\tau) = |c_0(\tau)|^2$, for $\epsilon = 1, 5, 7.5$ and 8. Initial condition: $c_0(0) = 1$, $c_n(0) = 0$ for (n > 0). Transition to quantum chaos corresponds to $\epsilon \approx 8$. Initial conditions as in Fig. 10.
- Fig. 12: Frequency Fourier spectrum of the quantum probability: $P_0(\tau) = |c_0(\tau)|^2$ for $\epsilon = 1, 5, 7.5$ and 8. Transition to chaos appears at $\epsilon \approx 8$. Initial conditions as in

Fig. 10.

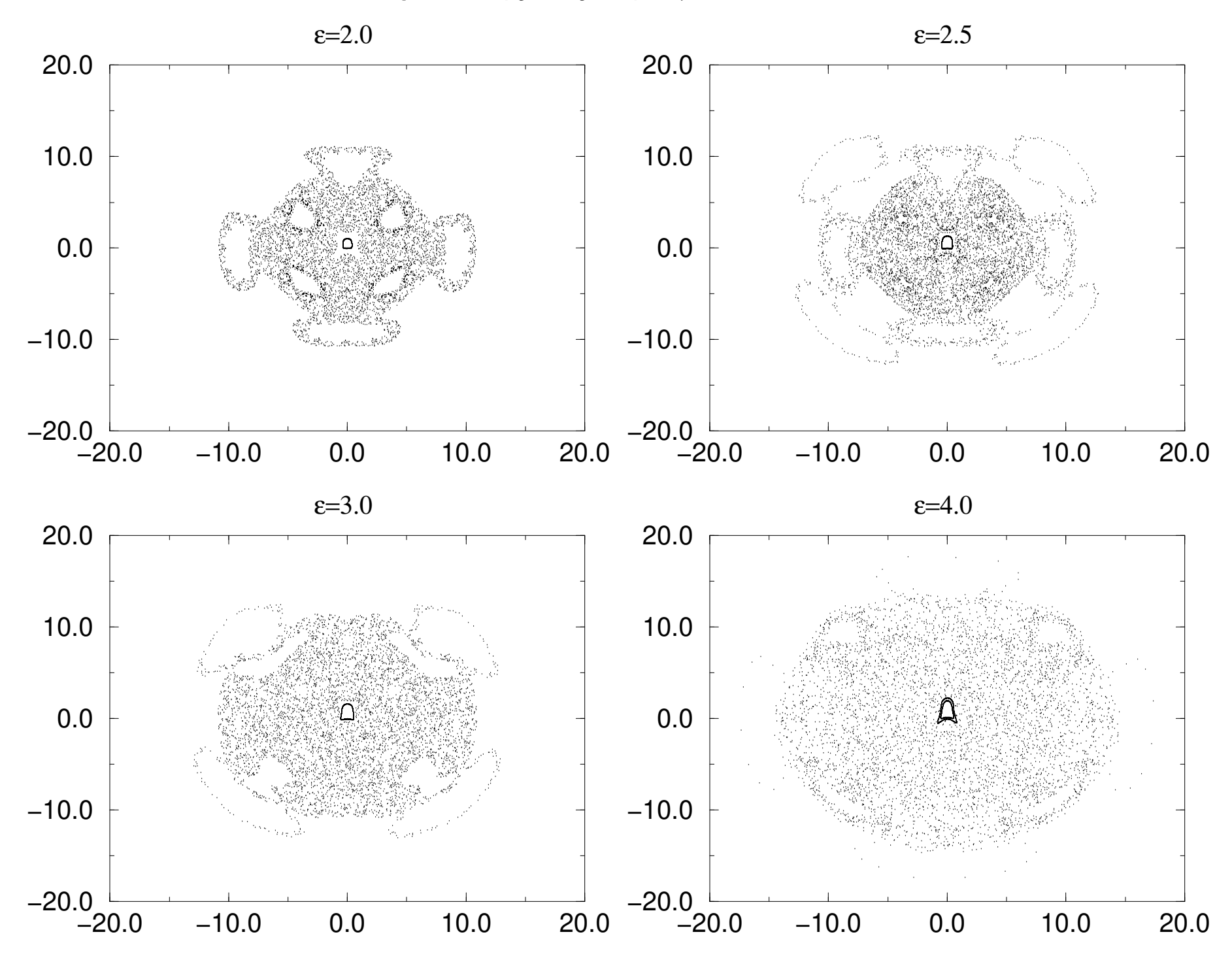
- **Fig. 13:** Dynamical evolution of the average value: $\langle \xi^2 \rangle \equiv \langle \Psi(\xi, \tau) | \xi^2 | \Psi(\xi, \tau) \rangle$, where the wave function $\Psi(\xi, \tau)$ is defined in (4.7). $\epsilon = 3, 5, 7.5$ and 8. Transition to chaos appears at $\epsilon \approx 8$. Initial conditions as in Fig. 10.
- **Fig. 14:** Frequency Fourier spectrum of the quantum amplitude: $\langle \xi^2 \rangle$, for $\epsilon = 1, 5, 7.5$ and 8 Transition to chaos appears at $\epsilon \approx 8$. Initial conditions as in Fig. 10.
- Fig. 15: Time evolution of two functions: the unperturbed Hamiltonian of quantum linear oscillator (4.3), $\langle \hat{\mathcal{H}}_{LO} \rangle$, and the amplitude $\langle \xi^2 \rangle$, for the values of the perturbation parameter $\epsilon = 0$, 0.5 and 2. The corresponding classical dynamics is regular in this case. $\epsilon = 0$, 0.5, 2. Initial conditions as in Fig. 10.
- Fig. 16: The time evolution of the same functions shown in Fig. 14 but for larger values of the parameter $\epsilon = 3$, 5, 7.5 and 8. The curves (3) and (4) correspond to the classically chaotic regime of motion. Initial conditions as in Fig. 10.



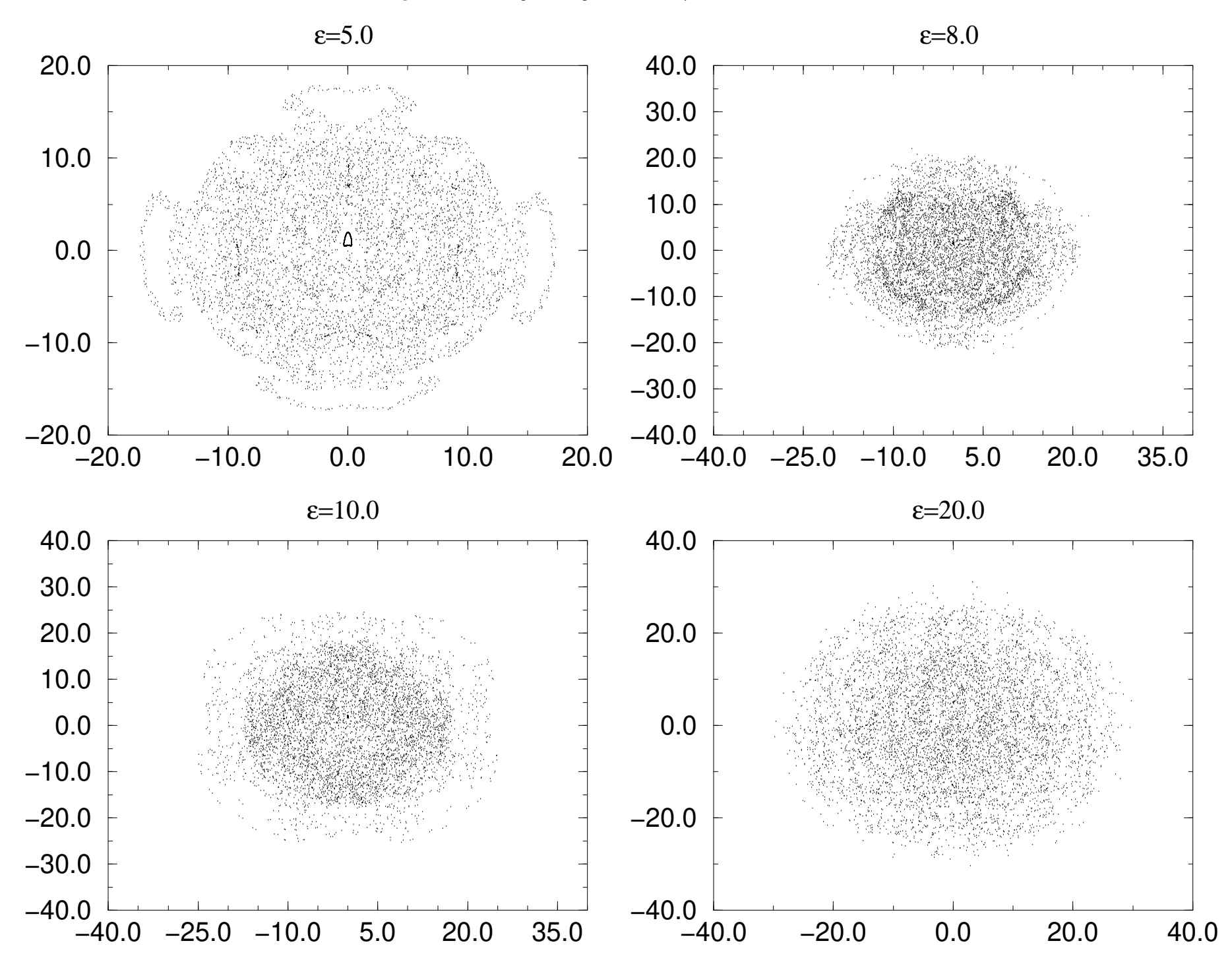




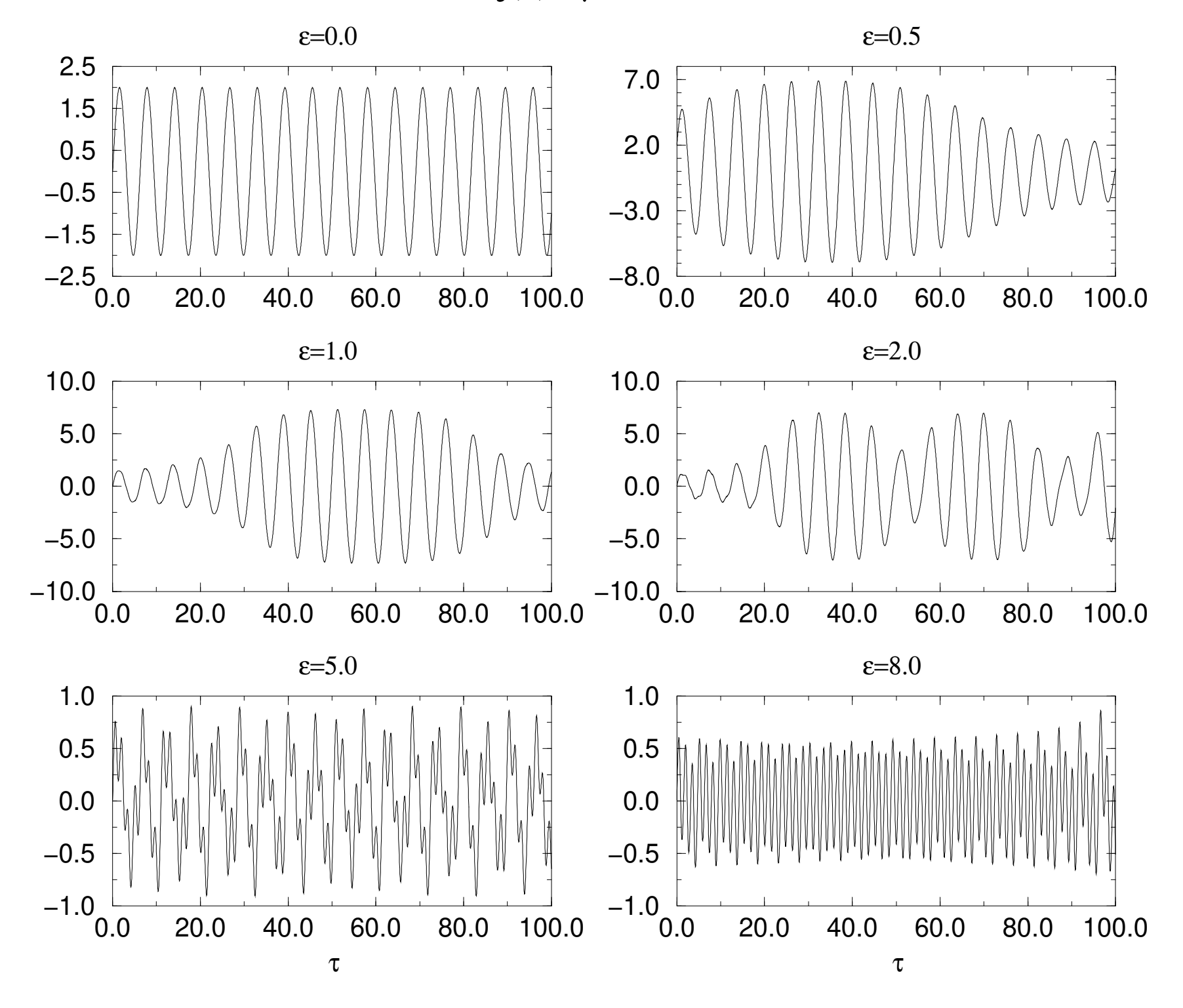
Phase Space (ξ , d ξ /dt); μ =3.99



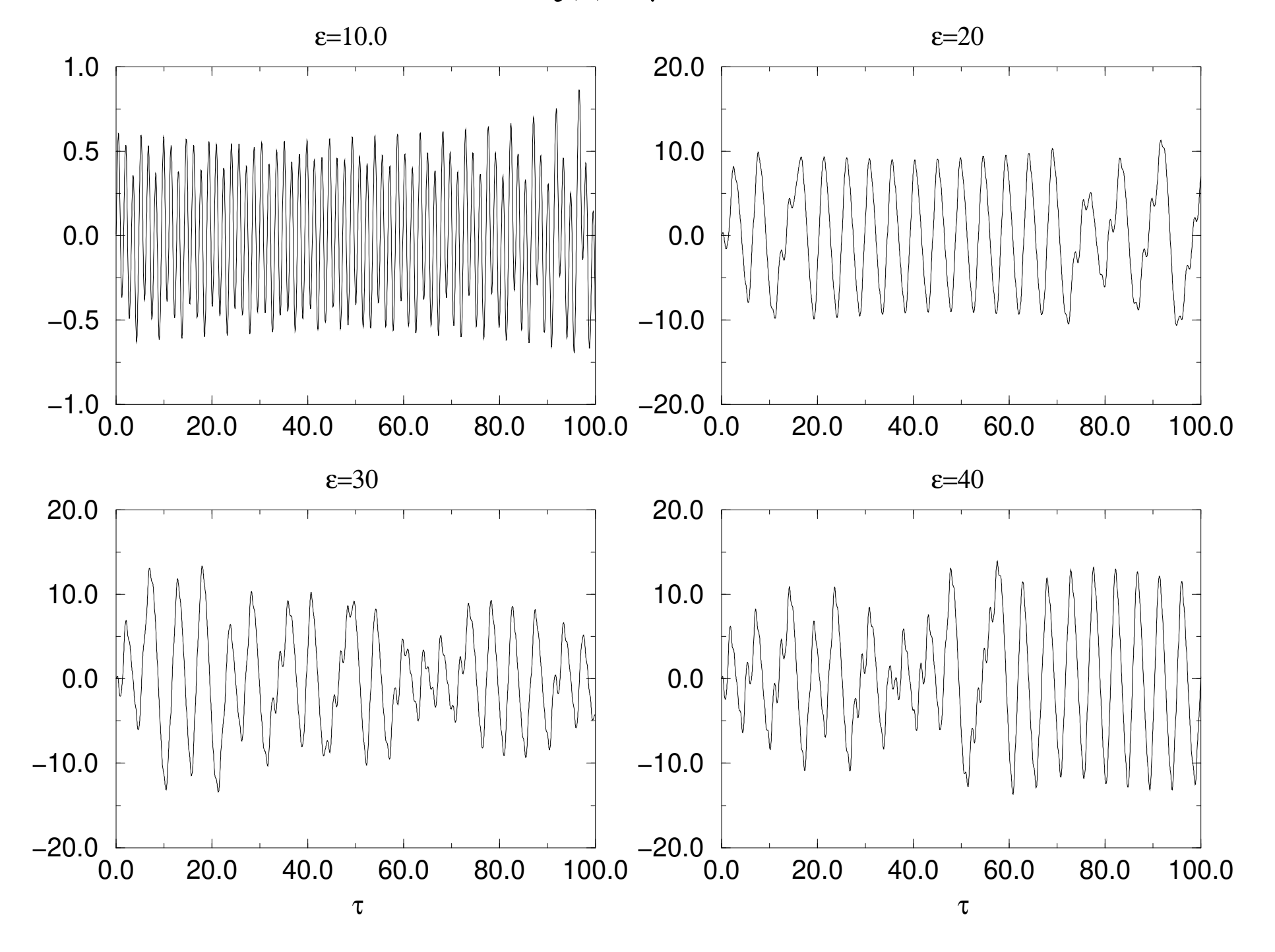
Phase Space (ξ , d ξ /dt); μ =3.99



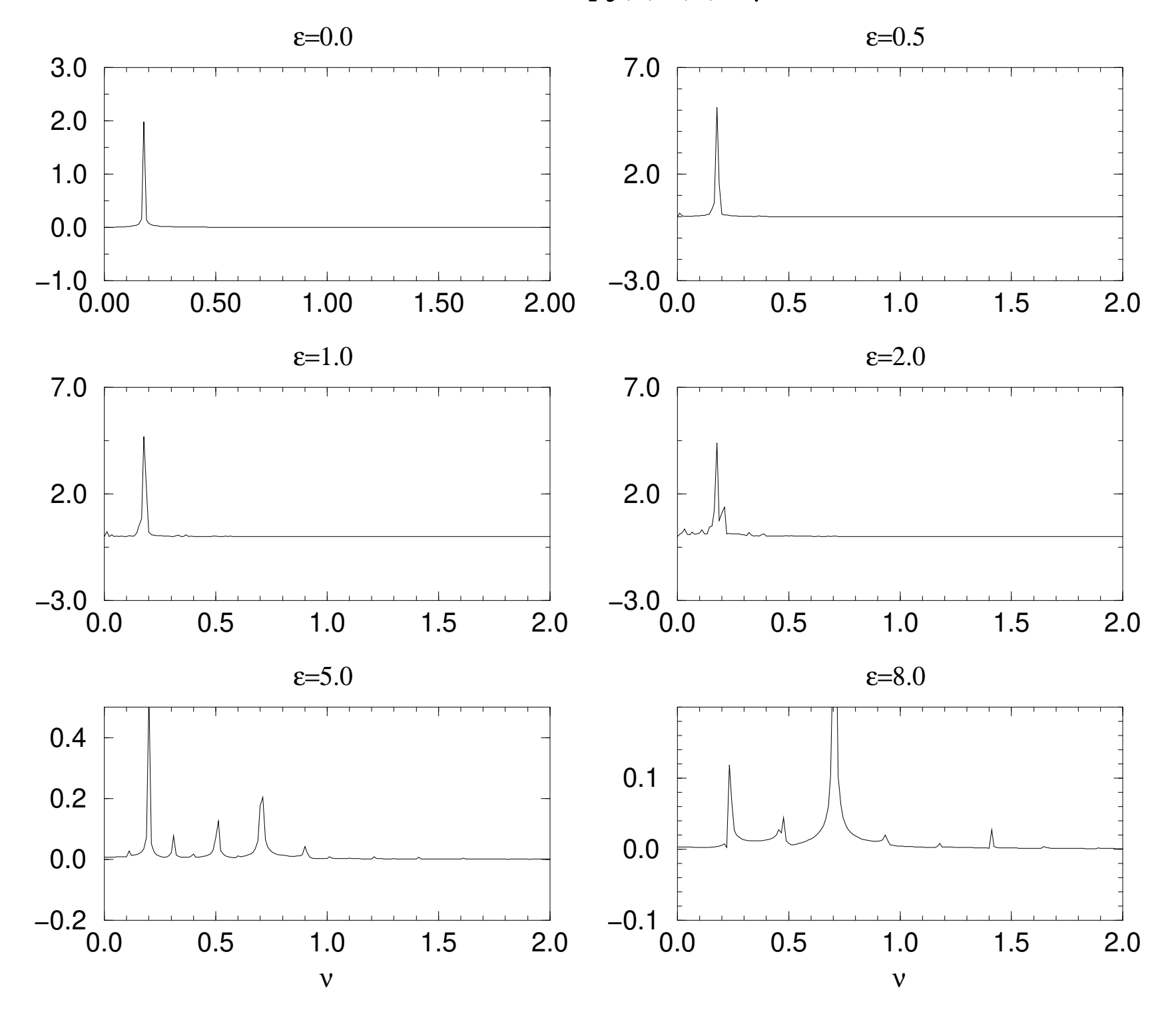
Evolution $\xi(\tau)$; μ =3.99



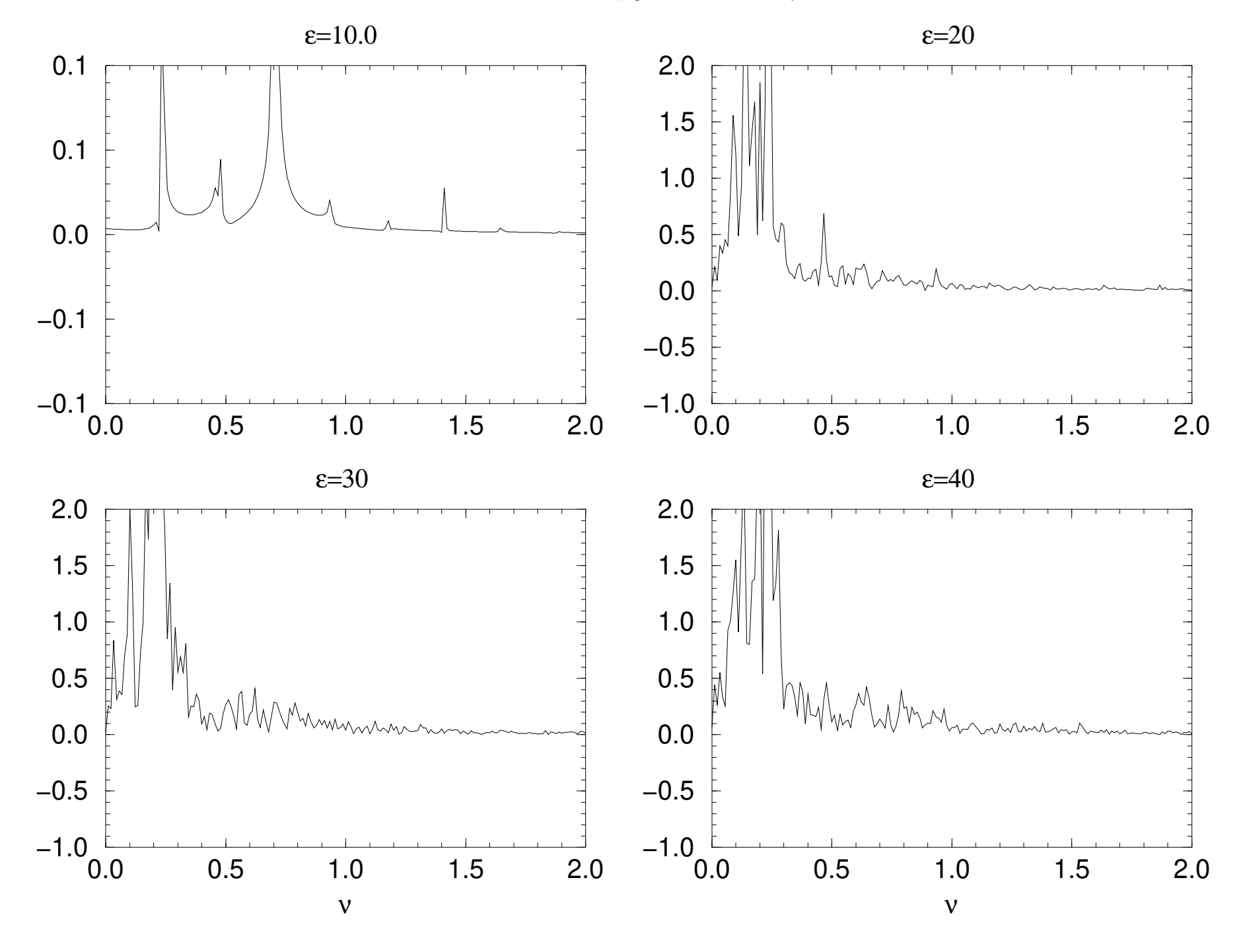
Time Evolution: $\xi(\tau)$; μ =3.99

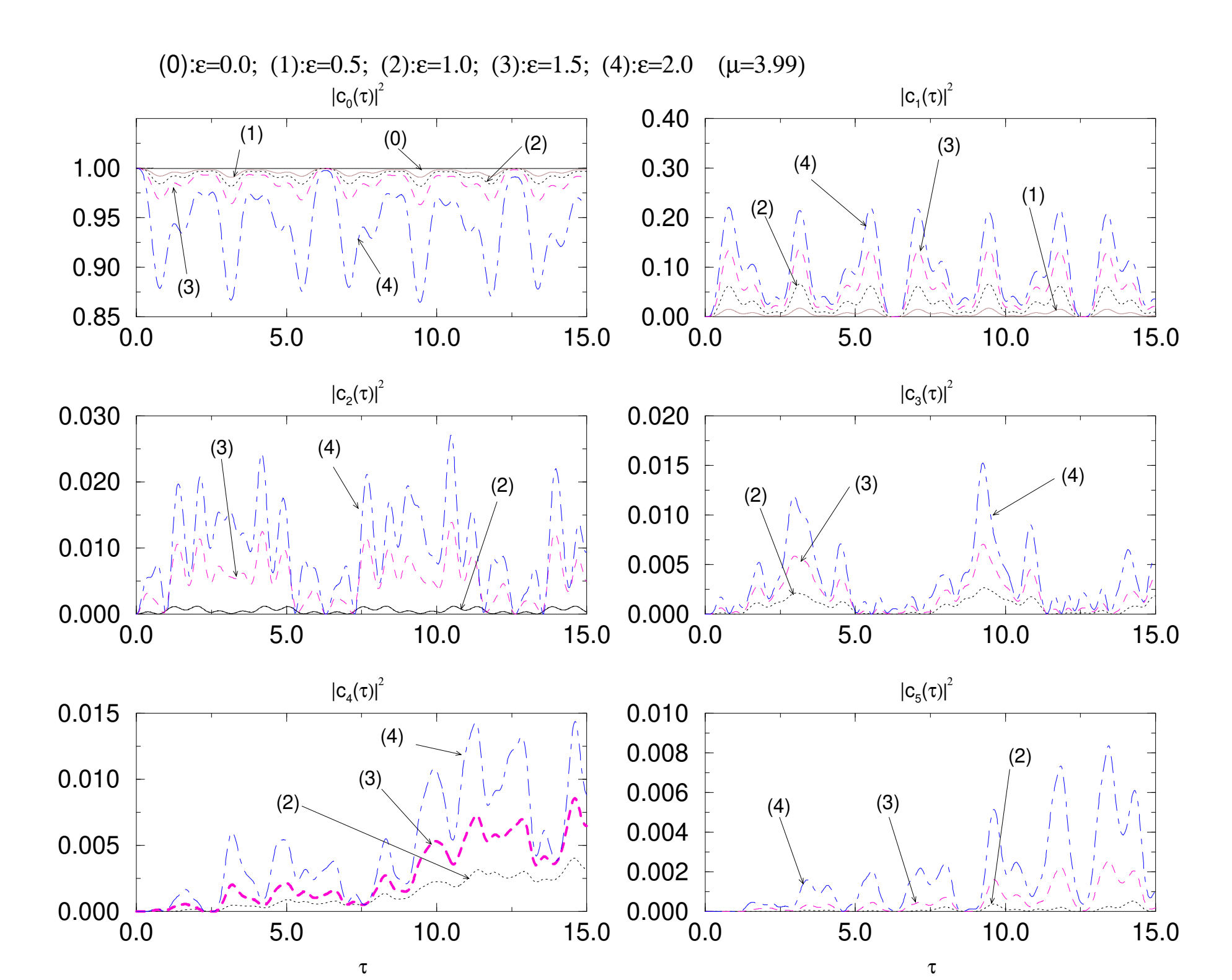


Fourier Transformation: Re F[$\xi(\tau)$](ν); μ =3.99



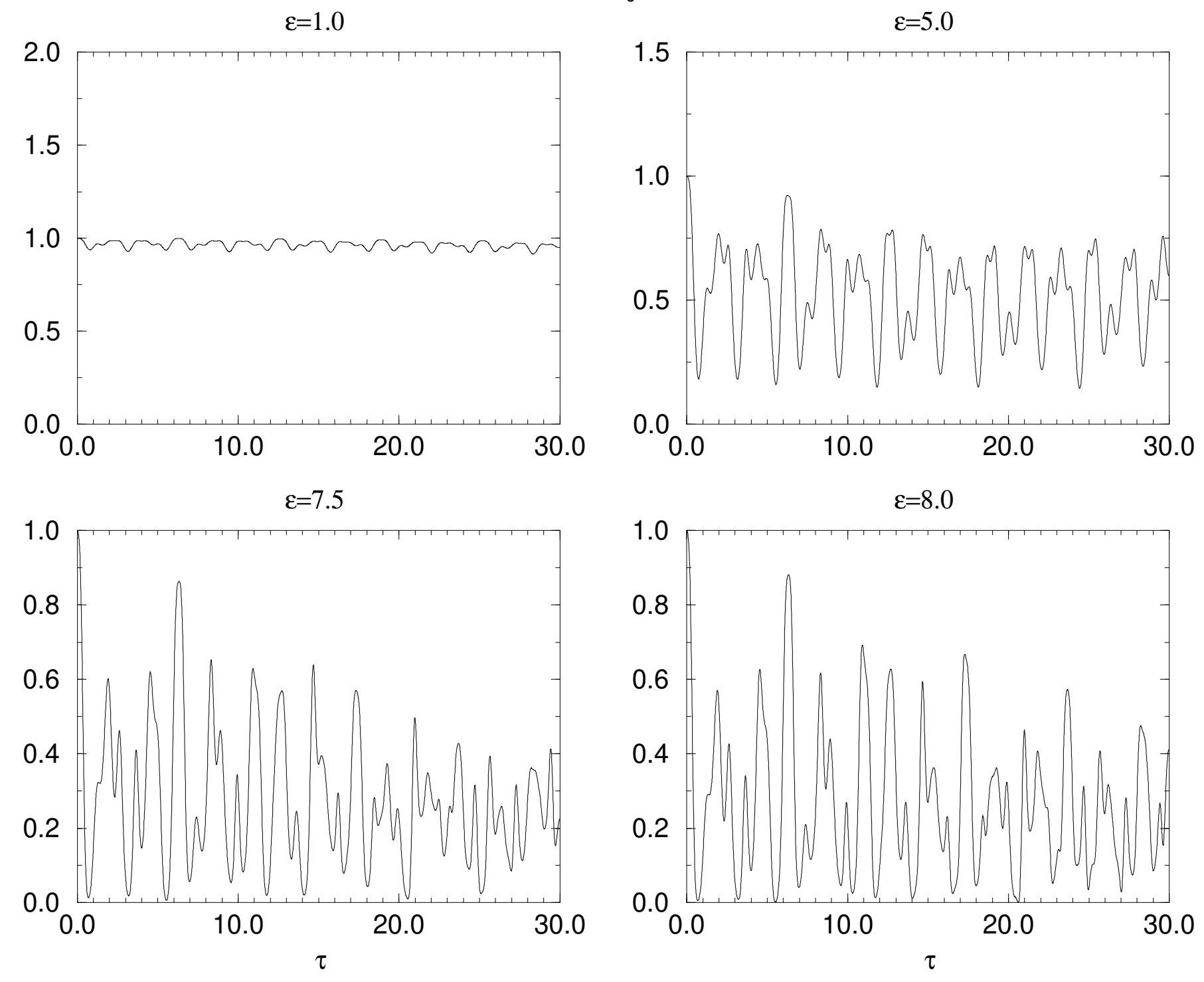
Fourier Transformation: Re F[$\xi(\tau)$](ν); μ =3.99



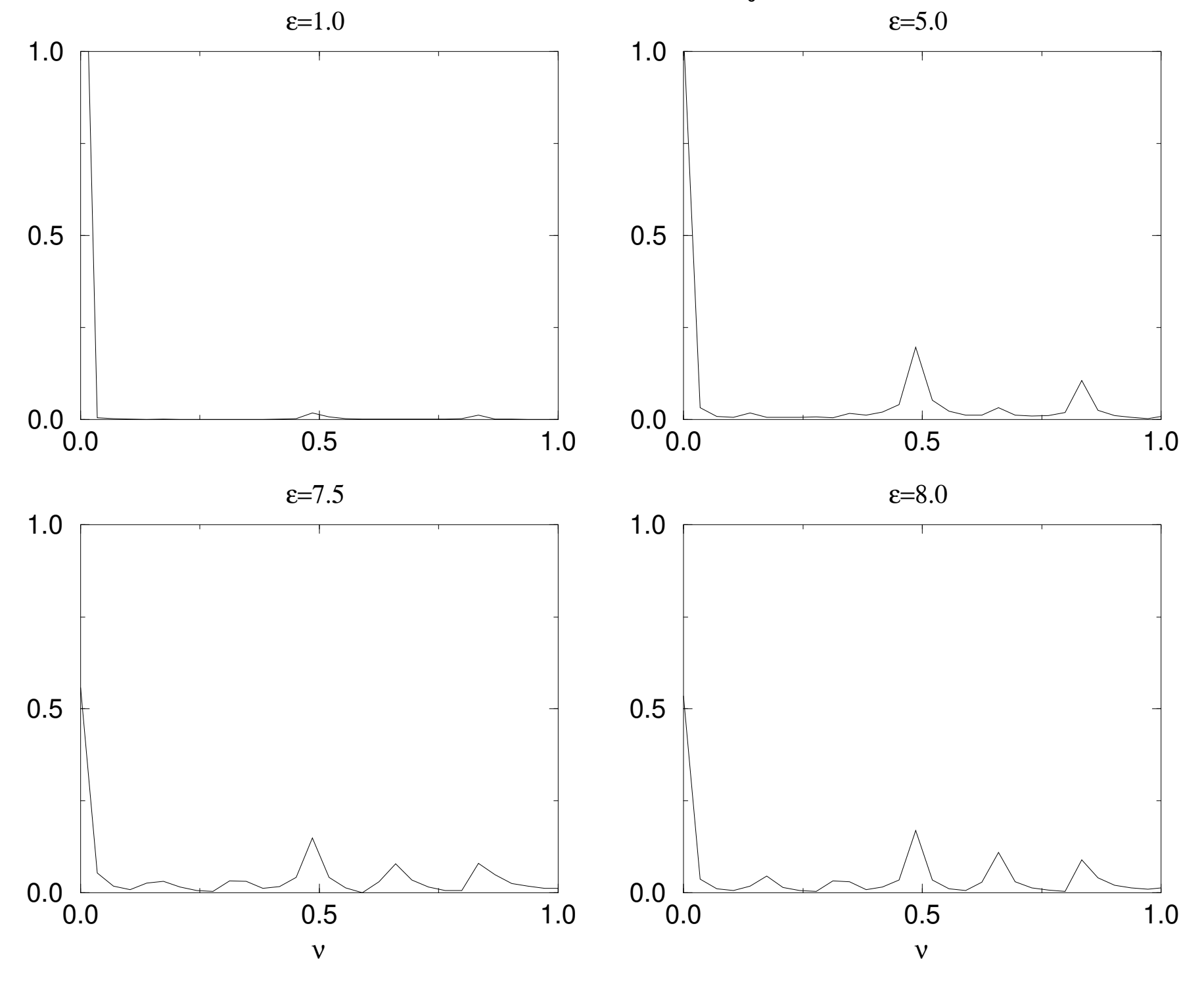


(1): ϵ =3.0; (2): ϵ =5.0; (3): ϵ =7.5; (4): ϵ =8.0 $\left|\mathbf{c}_{0}(\tau)\right|^{2}$ $\left|c_{1}(\tau)\right|^{2}$ 1.0 8.0 (1) (4) 0.6 (2) 0.5 0.4 0.2 (4) (3) (1) 0.0 0.0 (3) 3.0 5.0 2.0 3.0 5.0 2.0 4.0 1.0 4.0 1.0 $\left|c_{2}(\tau)\right|^{2}$ $\left|c_{3}(\tau)\right|^{2}$ 0.5 0.4 (3) (4) (4) 0.4 0.3 (3) 0.3 0.2 (1) 0.2 0.1 0.1 0.0 0.0 2.0 3.0 4.0 5.0 1.0 3.0 5.0 1.0 2.0 4.0 τ τ

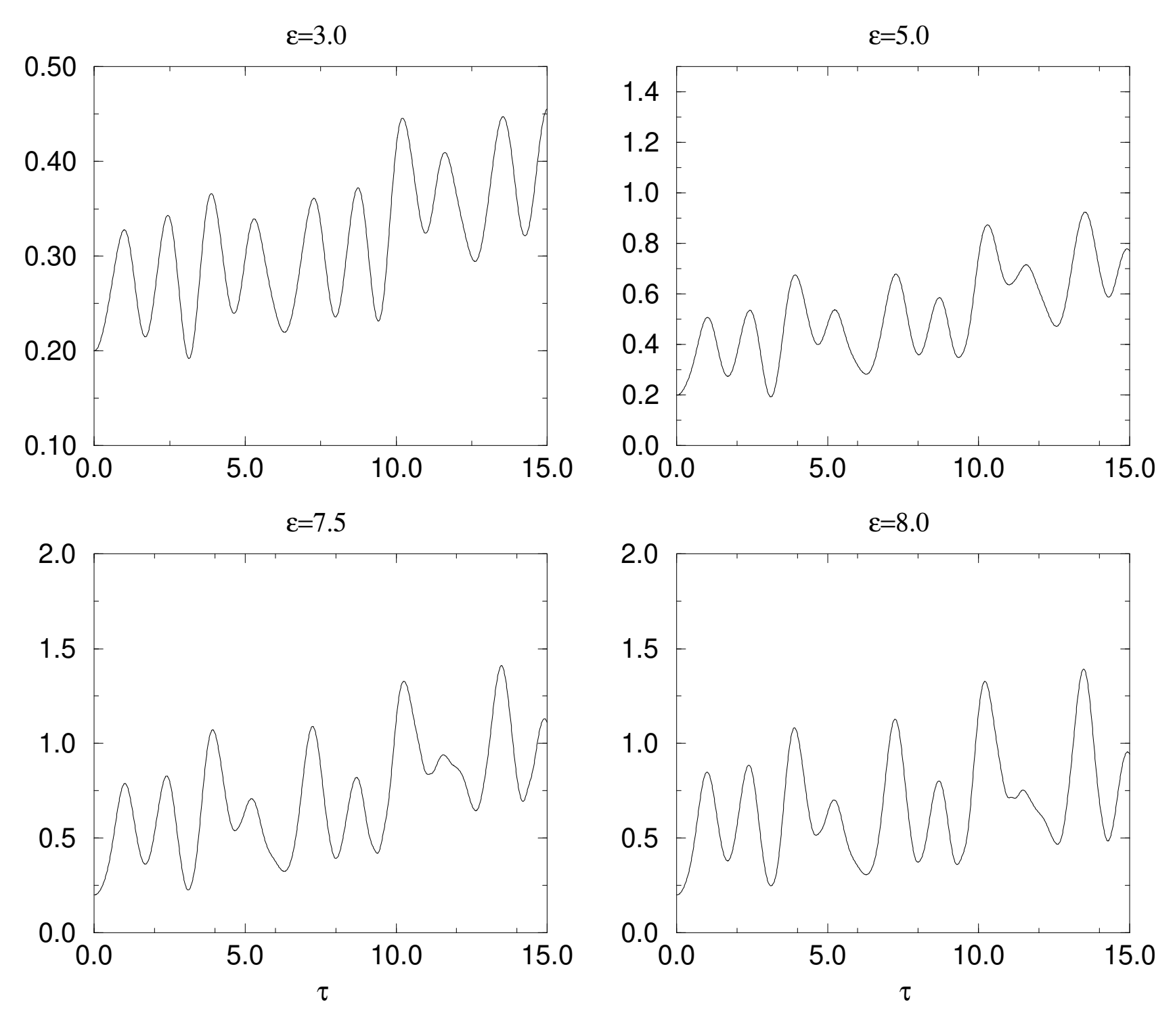
Evolution: $|c_0(\tau)|^2$



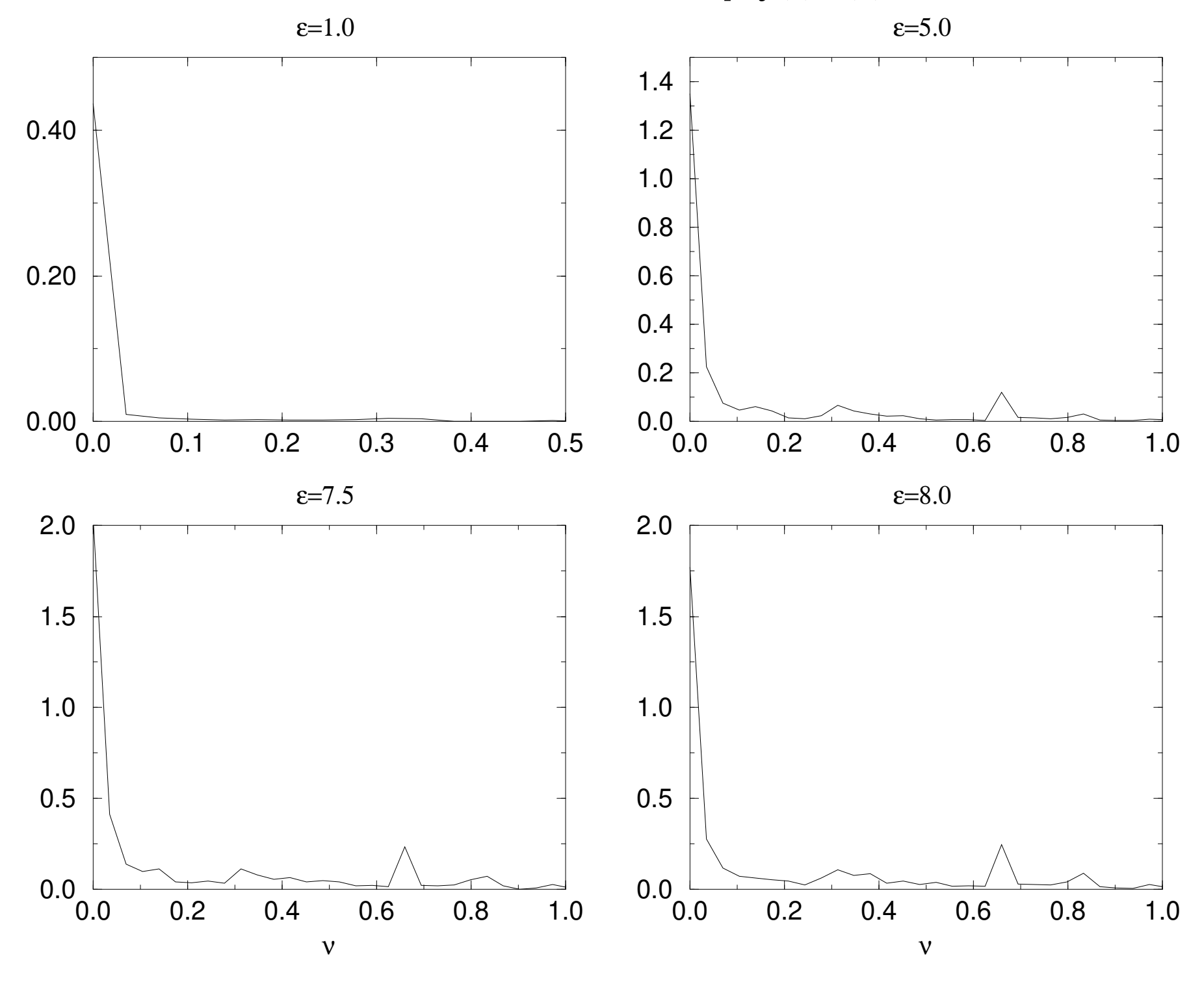
Fourier Transformation: Re $F[|c_0(\tau)|^2](v)$



Evolution: $\langle \xi^2 \rangle$



Fourier Transformation: Re $F[<\xi^2(\tau)>](v)$



 μ =3.99

